NASA CR-145354-1

Reduction of Computer Usage Costs in Predicting Unsteady Aerodynamic Loadings Caused by Control Surface Motions

Addendum to Computer Program Description

W.S. Rowe and J.R. Petrarca

Boeing Commercial Airplane Company
Seattle, Washington

Prepared for
Langley Research Center
under contract NAS1-14122

NASA
National Aeronautics and
Space Administration

1980

CONTENTS

REDUCTION OF COMPUTER USAGE COSTS IN PREDICTING UNSTEADY AERODYNAMIC LOADING CAUSED BY CONTROL SURFACE MOTIONS ADDENDUM TO COMPUTER PROGRAM DESCRIPTION

W. S. Rowe and J. R. Petrarca

SUMMARY

This document describes the changes to be made in NASA CR-145354 that will provide increased accuracy and increased user flexibility in prediction of unsteady loadings caused by control surface motions. Analysis flexibility is increased by reducing the restrictions on the location of the downwash stations relative to the leading edge and the edges of the control surface boundaries. Analysis accuracy is increased in predicting unsteady loading for high Mach number analysis conditions through use of additional chordwise downwash stations. User Guidelines are presented to enlarge analysis capabilities of unusual wing-control surface configurations. Comparative results indicate that the revised procedures provide accurate predictions of unsteady loadings as well as providing reductions of 40 to 75 percent in computer usage costs required by previous versions of this program.

INTRODUCTION

The computer program described in NASA CR-3009 and NASA CR-145354 was developed to reduce computer usage costs of a program (described in NASA CR-2543) developed to predict unsteady loadings on lifting surfaces that are caused by control surface motions.

The replacement program described in NASA CR-145354 does provide economical and accurate predictions of unsteady loadings for the sample cases evaluated in NASA CR-3009. However, it has been determined that the program is limited in its usefulness in analyses of very high aspect ratio wing-control surface configurations. It is also limited in predicting accurate unsteady loadings in high Mach number analyses.

The present report describes methods used to increase analysis capabilities by

1) reducing the restrictions on the location of downwash stations
2) increasing accuracy in high Mach number analyses
3) applying planform smoothing option to obtain converged solutions
4) applying non-standard downwash chord distributions in analyses of unusual configurations.

The present work represents an extension of previous methods described in NASA CR-3009 to provide a capability for obtaining economical and accurate predictions of unsteady loadings caused by control surface motions.

SOLUTION PROCESS AND PROGRAM LIMITATIONS

The solution process involved in predicting unsteady loadings on lifting surfaces is one of finding a set of pressure functions that satisfy the boundary value problem defined by the integral equation

$$\frac{w}{V} = \iint \Delta P(\xi,\eta)\ K(x,\xi,y,\eta)\ d\xi d\eta$$

having normalwash boundary conditions defined by

$$\frac{w}{V} = \frac{\partial z}{\partial x} + \frac{ikz}{b_0}$$

z ——— represents the motion description of the lifting surface

$\frac{w}{V}$ ——— kinematic normalwash representing the non-dimensional normalwash acting on the lifting surface

$K(x,\xi,y,n)$ —— is the kernel function representing the normalwash at x, y due to a pulsating pressure located at ξ,η

$\Delta P(\xi,\eta)$ —— is the unknown pressure distribution defined over the lifting surface.

A basic assumption applied to the solution process is to assume that the lifting surface pressure distribution may be represented by a linear combination of pressure distributions that satisfy the planform edge boundary conditions.

That is:

$$\Delta P(\xi,\eta) = a_1 \Delta P_1(\xi,\eta) + a_2 \Delta P_2(\xi,\eta) + \ldots + a_n \Delta P_n(\xi,\eta)$$

Based on this assumption, a set of theoretical downwash distributions is calculated for each of the assumed pressure distributions using the integral equation

$$\frac{w}{V_i} = \iint \Delta P_i(\xi,\eta)\ K(x,\xi,y,\eta)\ d\xi d\eta$$

The kinematic downwash is set equal to the sum of downwashes generated (for each of the assumed pressure distributions) at n downwash stations.

$$\begin{vmatrix} \frac{w}{V_1} \\ \frac{w}{V_2} \\ \vdots \\ \frac{w}{V_n} \end{vmatrix} = \begin{bmatrix} \frac{w}{V_{1,1}} & \frac{w}{V_{1,2}} & \cdots & \frac{w}{V_{1,n}} \\ \frac{w}{V_{2,1}} & \frac{w}{V_{2,2}} & \cdots & \frac{w}{V_{2,n}} \\ \vdots & \vdots & & \vdots \\ \frac{w}{V_{n,1}} & \frac{w}{V_{n,2}} & \cdots & \frac{w}{V_{n,n}} \end{bmatrix} \begin{vmatrix} a_1 \\ a_2 \\ \vdots \\ a_n \end{vmatrix}$$

kinematic downwash — theoretical downwash — unknown coefficient

The unknown coefficients are evaluated by a standard matrix inversion process. The individual coefficients define how much of each downwash sheet (developed for each assumed pressure mode) is required to satisfy the kinematic downwash boundary condition.

The final pressure distribution is then obtained by inserting the known coefficient multipliers into the pressure series

$$\Delta P(\xi,\eta) = a_1 \Delta P_1(\xi,\eta) + a_2 \Delta P_2(\xi,\eta) + \ldots + a_n \Delta P_n(\xi,\eta)$$

This method will produce reasonable solutions provided the kinematic downwash distribution is smooth and continuous. It is also assumed that a sufficient number of downwash matching stations is used to accurately define the kinematic downwash distribution and that the generated downwash sheets are accurately calculated.

It should be noted that smooth and continuous assumed pressure distributions will only provide smooth and continuous downwash distributions. Thus, if the kinematic downwash distribution is not smooth and continuous (such as defined for a wing having a moving control surface) the use of smooth and continuous theoretical downwash distribution to represent a discontinuous downwash distribution would be highly dependent on the number of downwash sheets used as well as on the location of the downwash matching stations distributed over the surface.

The solution process applied in the present method to obtain converged solutions for lifting surfaces having discontinuous downwash distributions is described in NASA CR-3009. The schematic shown in figure 1 indicates the method used in analyses of lifting surfaces having discontinuous downwash distributions.

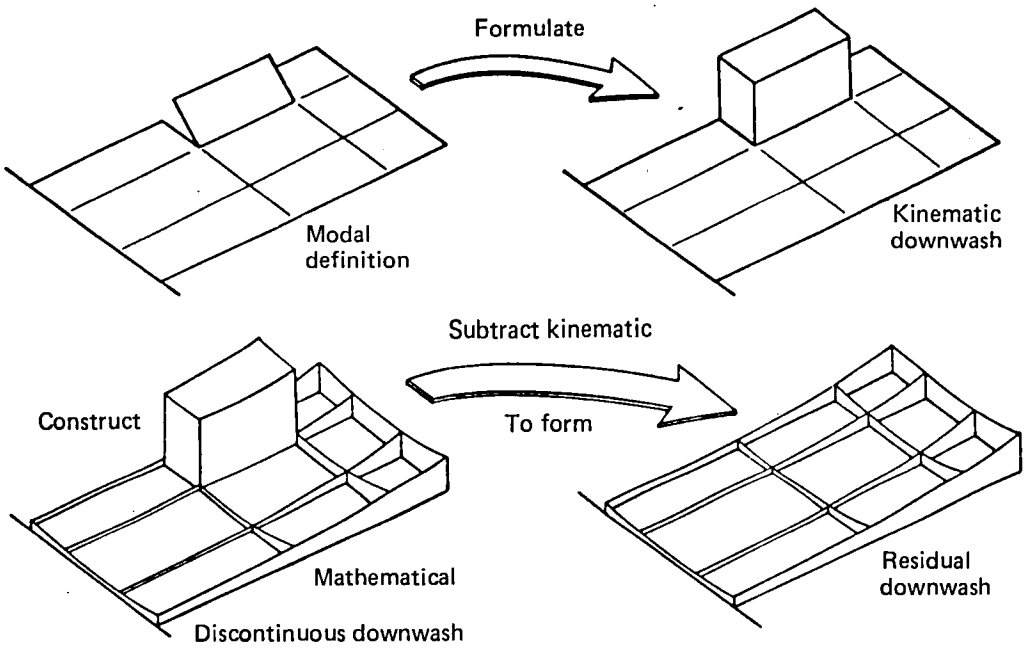

Figure 1.—Solution Process Applied to Trailing Edge Control Surface Analysis

The solution process is given as

1. define the kinematic downwash distribution from the motion definition

2. calculate a theoretical downwash distribution that contains identical downwash discontinuities as contained in the kinematic distribution (using pressure expressions developed in NASA CR-3009)

3. subtract the theoretical discontinuous downwash distribution from the kinematic distribution, forming a new distribution that is smooth and continuous (residual downwash).

4. obtain standard lifting surface solutions of a new boundary value problem that has downwash boundary conditions defined by the residual distribution from step 3.

5. calculate the final pressure distribution by summing the pressures required to remove the downwash discontinuities and the pressures obtained from step 4.

This procedure will provide accurate predictions of unsteady pressure distributions over lifting surfaces having oscillating control surfaces provided if a sufficient number of downwash matching stations are used and if the theoretical downwashes are accurately calculated at the downwash matching stations.

Numerical investigations indicate that accurate calculations of theoretical downwashes are readily obtained for collocation stations (downwash matching stations) located outside of the leading edge region and at large distances from the control surface edges. However, the previous version of the program contained a restriction prohibiting the placing of collocation points within .02S or less from the leading edge or from control surface edges. This restriction severely impairs user flexibility in using this program for analysis of high aspect ratio wing control surface configurations. Consequently, extensive modifications have been made in chordwise and spanwise integration routines to reduce the size of the restricted regions to allow greater user flexibility in analysis of high aspect ratio configurations.

Figure 2 represents a typical wing control surface configuration and indicates the regions where additional spanwise and chordwise integration stations have been introduced to provide more accurate downwash calculations. It should be noted that the troublesome regions adjacent to control surface boundaries extend from .02S ahead to .03S aft of the hingeline. The spanwise region difficulty extends for a distance of .02S from control surface side edges.

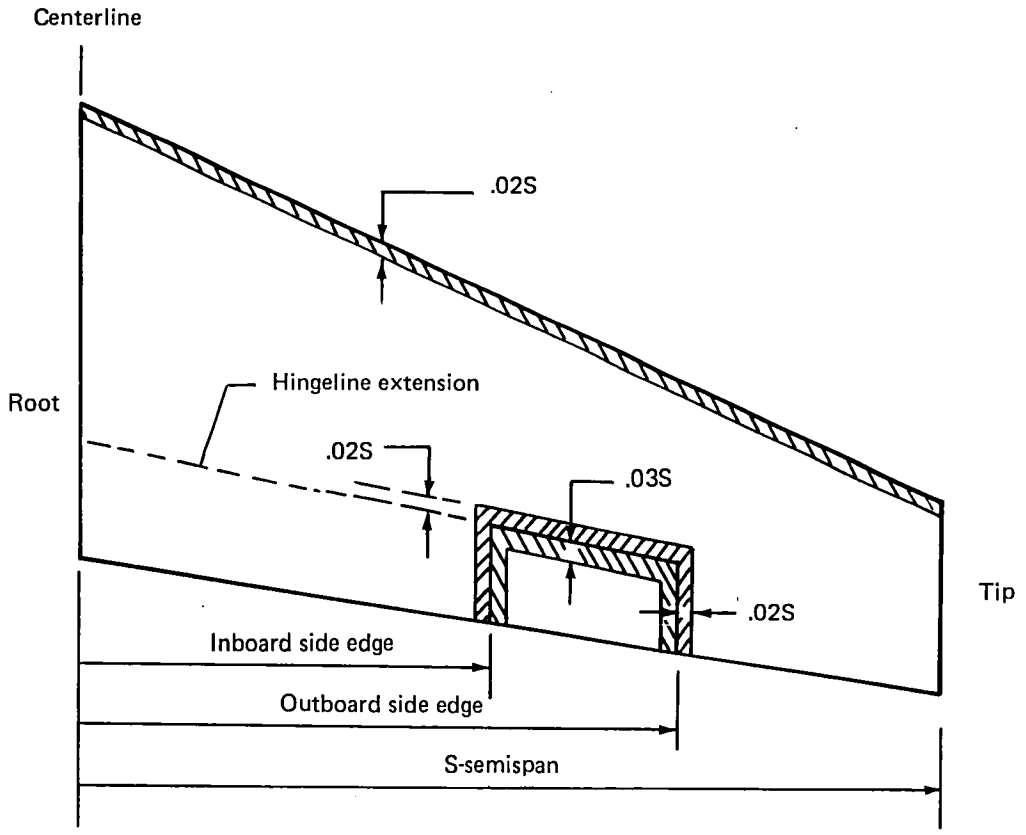

Figure 2.—Typical Analysis Planform Displaying Regions Requiring Special Integration Procedures

Accurate downwashes are calculated for downwash stations located in the troublesome regions, however, there is a substantial increase in computer usage costs as the downwash station approach control surface boundaries. For example the computer usage costs for computing a single value of downwash at a station downstream of the .03S hingeline boundary is .660 CPU sec per downwash station. If the downwash station is located between .01S and .03S downstream of the hingeline, required computer time is 1.161 CPU sec per downwash station. If the downwash station is located between .0016S and .01S from the hingeline the costs become 1.473 CPU sec per downwash station.

Note that downwash stations are not permitted within .0016S from the hingeline.

If the downwash station is located between .005S and .02S from control surface side edges the computer time requirements become .989 CPU sec per downwash station.

Thus, computer usage costs are highly dependent upon configuration and on distribution of downwash stations relative to control surface boundaries.

Numerical investigations have been performed to check the continuity of calculated residual downwashes in the vicinity of control surface boundaries. Figure 3 represents a typical planform that was used to check downwash continuity across the hingeline

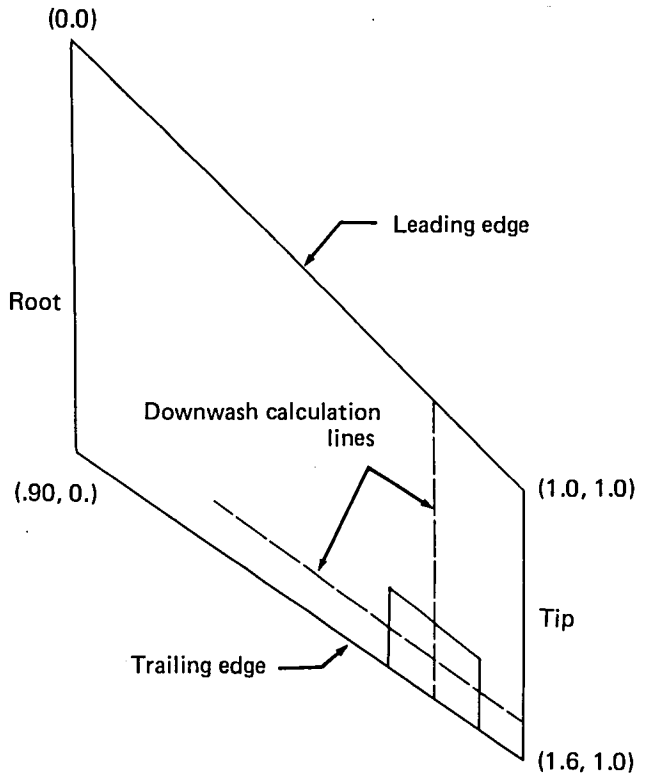

Figure 3.—Analysis Configuration of Downwash Continuity Study

and control surface side edges. Figure 4 and figure 5 represent real and imaginary part of the residual downwash distribution along a streamwise ray that crosses the hingeline. The downwashes are smooth and continuous for all stations located at a distance greater than .0016S from the hingeline. The numerical integration procedures are not sufficiently accurate to provide reasonable calculations of downwashes for stations closer than .0016S from the hingeline. Thus, if a downwash station is inadvertently located within a distance of .0016S from the hingeline the program will print out a warning to alert the user that possible inaccuracies may result in using the prescribed downwash station locations.

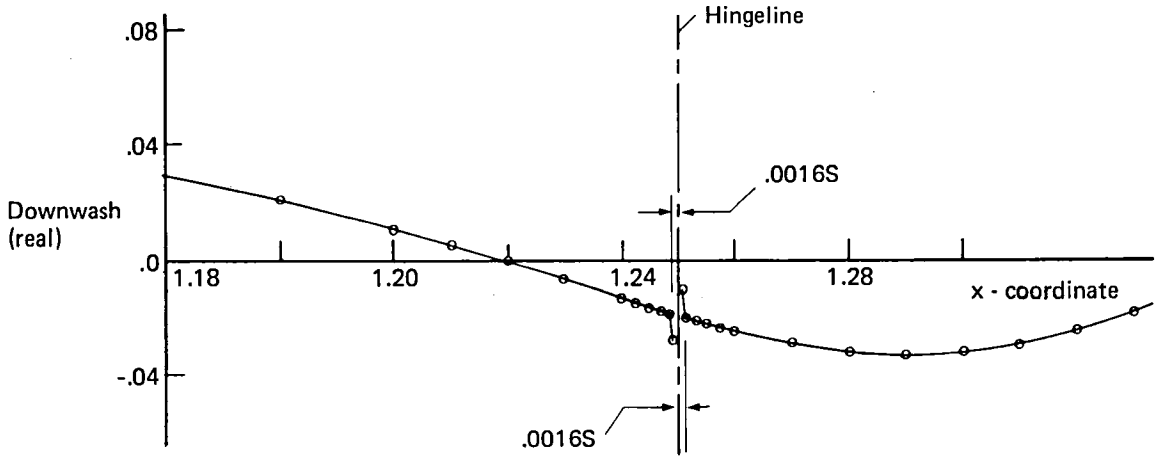

Figure 4.—Real Part of Residual Downwash Across Hingeline; k = 1., M = .8

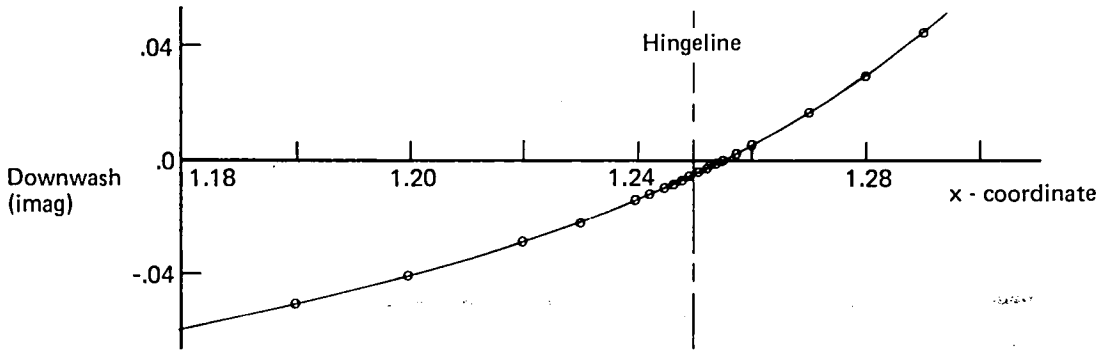

Figure 5.—Imaginary Part of Residual Downwash Across Hingeline; k = 1., M = .8

Figure 6 and figure 7 represent the real and imaginary parts of the residual downwash distribution for a ray that is parallel to the hingeline and crossing both side edges. The residual downwashes are smooth for all regions outside of .005S from the side edges. The downwash calculations tend to become inaccurate for stations located closer to the side edge than .005S. Consequently, a warning will be printed out to alert the user that possible inaccuracies may result if the downwash station locations defined by user input are closer to the side edge than .005S.

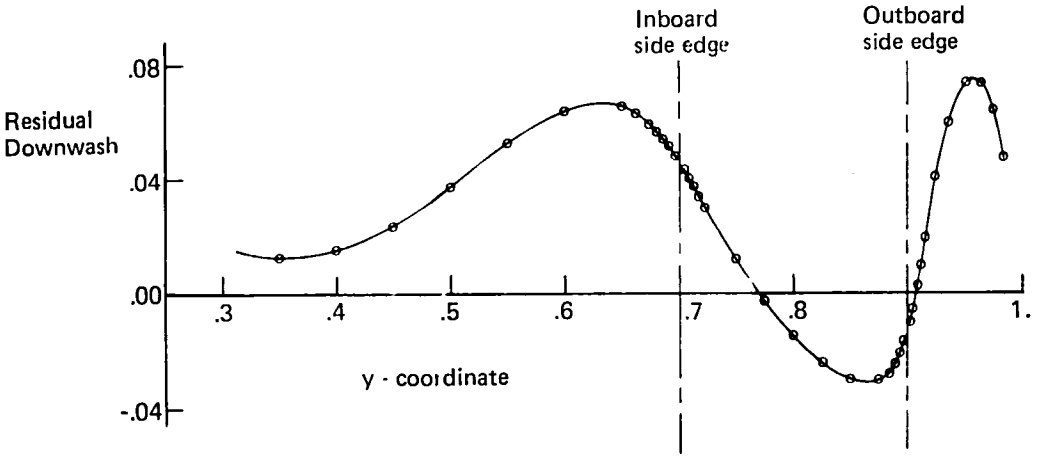

Figure 6.—Real Part of Residual Downwash Across Control Surface Side Edges for k = 1., M = .8

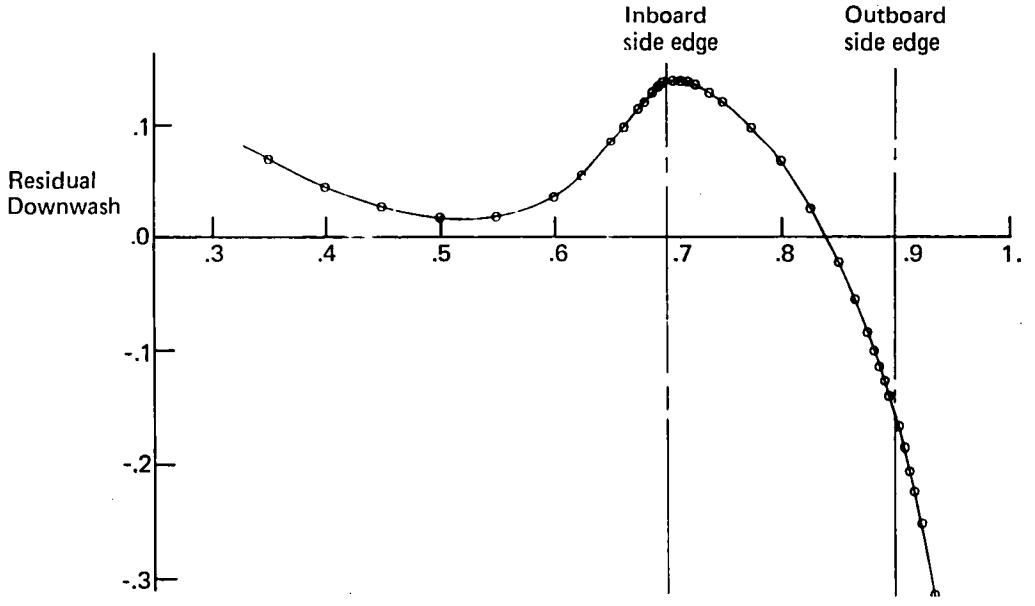

Figure 7.—Imaginary Part of Residual Downwash Across Control Surface Side Edges for k = 1., M = .8

Thus, the change in numerical integration procedures (in both the chord and span directions developed to provide accurate downwash calculations) allows greater user flexibility in locating the downwash stations in the vicinity of control surface boundaries than that available in previous versions of this program.

Extensive revisions have been made in the integration routines that are used to calculate downwashes for main surface solutions. This revision was developed to remove previous program limitations that only allowed a maximum of eight downwash stations distributed on each downwash chord. This program limitation severely affects analysis capability in predicting unsteady loadings of plate-type camber bending motion and limits accurate predictions of unsteady loadings in high Mach number analyses.

Downwash distributions obtained using the revised integration procedures for the high aspect ratio planform of figure 8 are shown in figure 9.

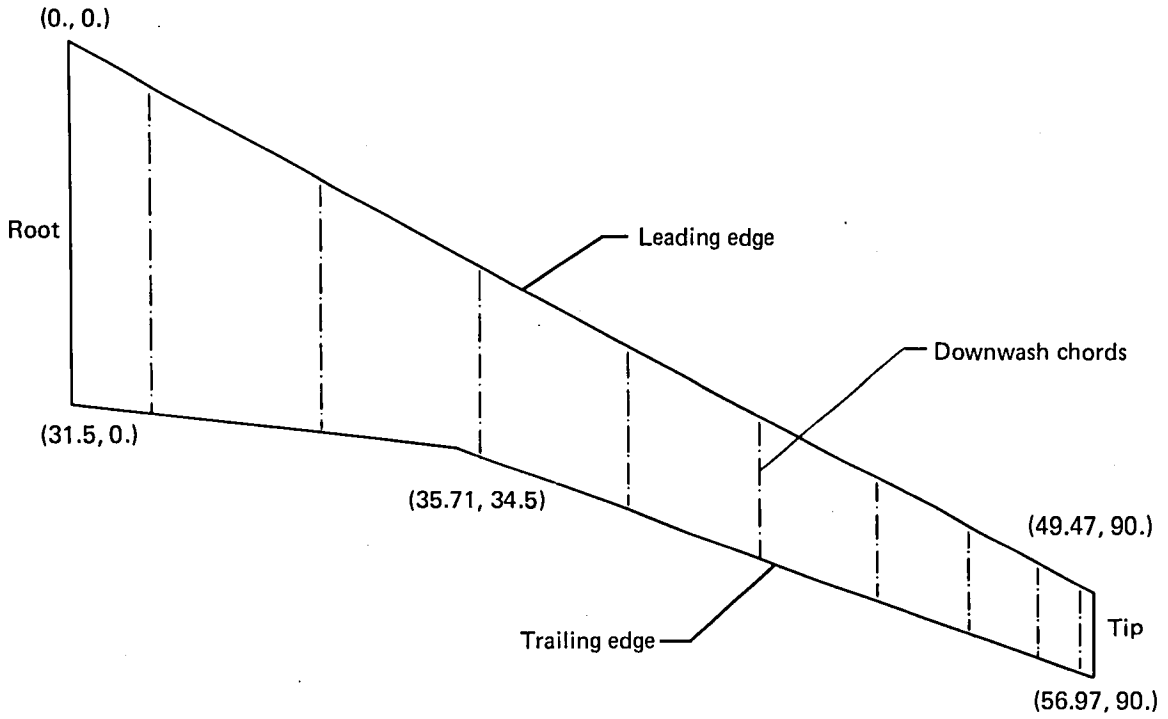

Figure 8.—Planform Used to Evaluate Downwash Distribution Generated in Main Surface Analysis

Figure 9 represents the theoretical chordwise downwash distribution calculated using the first pressure mode that is assumed to be distributed over the lifting surface.

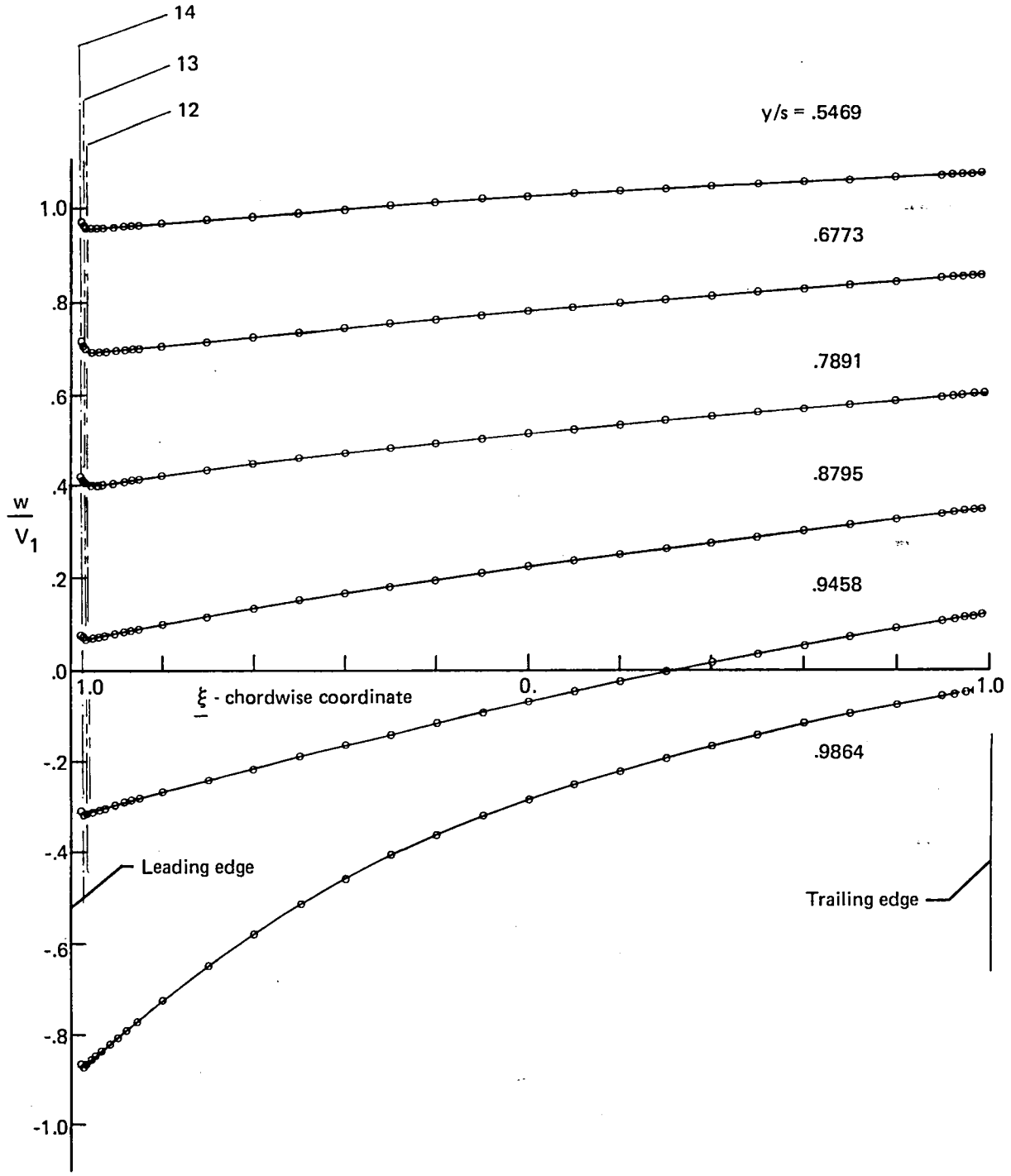

Figure 9.—Chordwise Downwash Distribution Obtained for First Assumed Pressure Mode of Main Surface Analysis

The numbers 12, 13 and 14 indicate the location of the first chordwise downwash station nearest the leading edge in a 12, 13 or 14 point downwash station per chord analysis. Where the chordwise location of the downwash stations are defined as

$$\underline{\xi} = -\cos(2i\pi/(2N + 1))$$

N is the total number of downwash stations.

The downwash distributions are smooth and continuous for all stations except the first station of 13 and 14 point per chord distribution. Consequently, the limitation on the number of downwash stations that may be distributed on each downwash chord has been revised upward from 8 to 12 points per chord.

The maximum number of downwash stations that may be distributed over the surface has been increased from 72 to 180.

NOTICE OF INOPERATIVE PROGRAM OPTIONS AND OTHER ERRATA

The program options of defining control surface rotations as such, using CRI in RHOF namelist, and CCR or DZDX in RHOG namelist is not operative (see pages 50, 51). Corrections of other errata in CR-145354 are as follows:

Page 18, line 17: $W = (w/V)/e^{i\omega t}$

Page 22, sec. 3.3: The RHOIV program loads under a field length of 65700_8 . . .

Page 22, sec. 3.3: Omit the third paragraph. The following sentence begins;

"The requirement for all other sections . . ."

Page 23: Following item 20 add:

21. NPDWC Number of points per downwash chord

Page 24, 25: The memory requirements are corrected to:

I.	Input Preparation	56000_8+ . . .
II.	Result preparation	55000_8+ . . .
IV.	C-matrix calculation	66000_8+ 10 * NPTRM * NPDWC
VII.	Results	45000_8
VIII.	Interpolated modes Output	50000_8+ . . .

Page 29, Word 1, line 2: Bits 17-00

Page 48, Card set 4: Exchange variable names PCMPRT and CMPRT

Page 48, Card set 5A, In the description of variable NDWC: $0 < NDWC*NPDWC \leqslant 180$.
Correct spelling from XPWD to XDWP.
In the description of NPDWC, $0 < |NPDWC| \leqslant 12$

Page 49, Card set 5A: In the note (1) correct to ". . . ($\underline{\eta}$ = .01, .1, . . .)"

Page 50, Card set 7A: Change variable ZF to ZF, ZSCALE. They are interchangeable.

HIGH MACH NUMBER–HIGH k VALUE ANALYSES

Accurate predictions of unsteady loadings become increasingly difficult for high Mach number analyses with an increasing value of reduced frequency. Standing waves develop in the kernel function in the region that significantly affects the calculation. Waves from pressure disturbances slowly move forward in unsteady flow as the sonic speed is approached or as the parameter $kM/(1 - M^2)$ becomes large. A graphical display of this phenomena is shown in figure 10 which represents a plot of the nonsingular part of kernel functions at M = .9 for various values of reduced frequency.

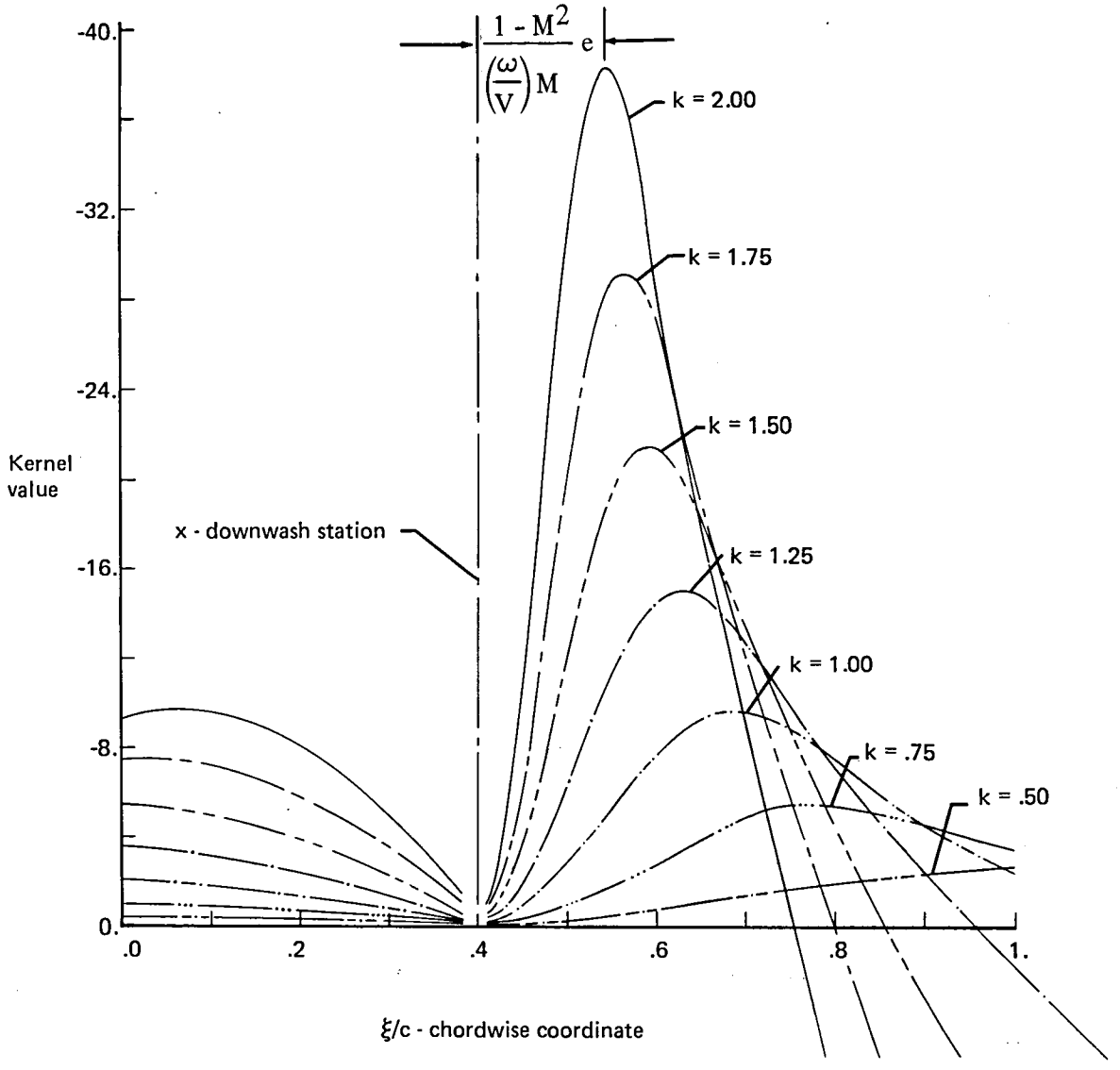

Figure 10.—Real Part of the Nonsingular Kernel Function; M = .9, y - η = .4572

The kernel function defines the downwash at "x, y" due to a unit pressure pulse located at "ξ,η". Location of the peak magnitude of the kernel function relative to the downwash station is given by the equation

$$\Delta\xi = \frac{1 - M^2}{\left(\frac{\omega}{V}\right)M} e$$

$$e = 2.71828...$$

Downwash sheets generated for high Mach number - high k value analyses tend to become very wavy which requires the generation and use of many downwash sheets to satisfy downwash boundary conditions.

Results of numerical investigations conducted on a rectangular wing of aspect ratio 4.67 to evaluate solution convergence are shown in figure 11.

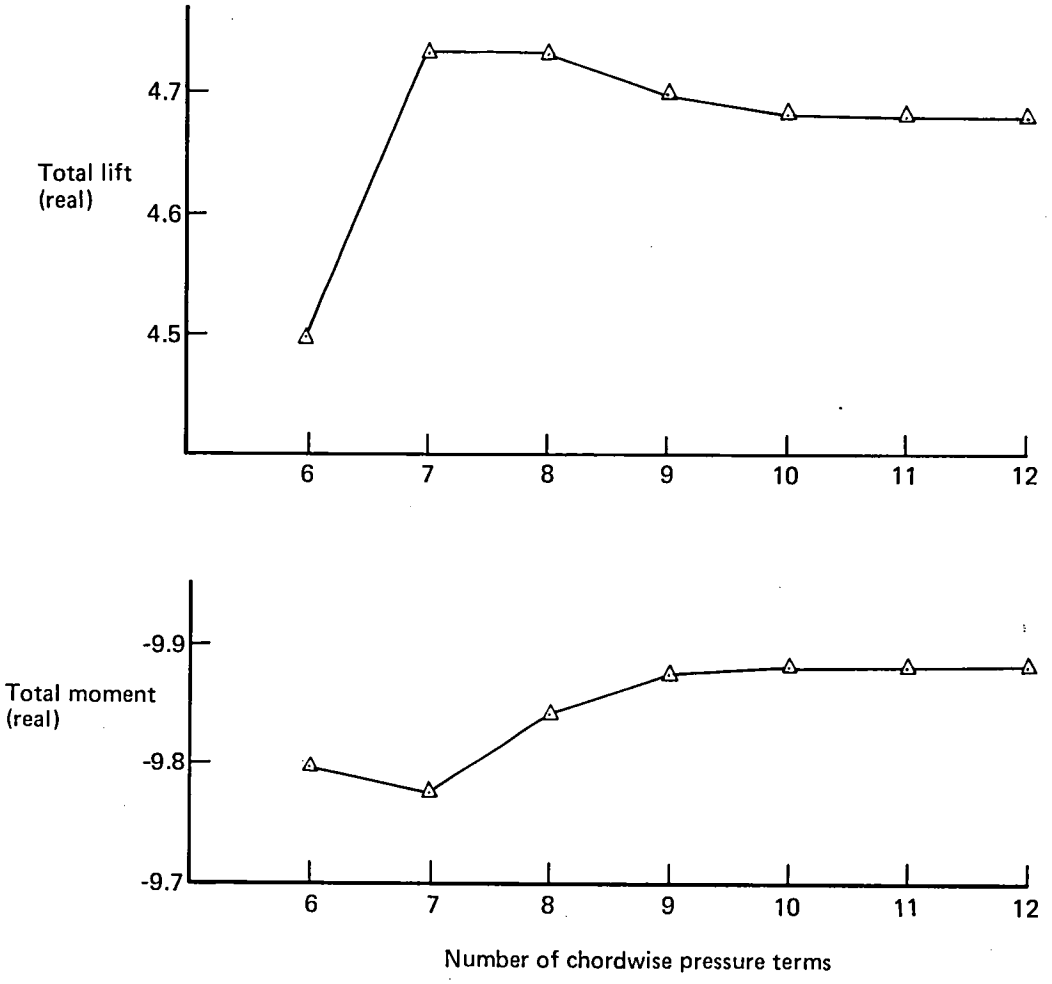

Figure 11.—Total Lift and Moment on a Rectangular Wing Due to Plunging Motion as a Function of Chordwise Pressure Terms for k = 2.0, M = .8

The lifts and moments represent total surface values. The results indicate that asymptotic solution values are achieved using 10 or more chordwise pressure terms for this particular analysis configuration that has a reduced frequency of k = 2.0 and Mach number of M = .8.

Results of investigations conducted to evaluate the waviness of chordwise pressures caused by large values of the parameter $kM/(1 - M^2)$ are shown in figure 12.

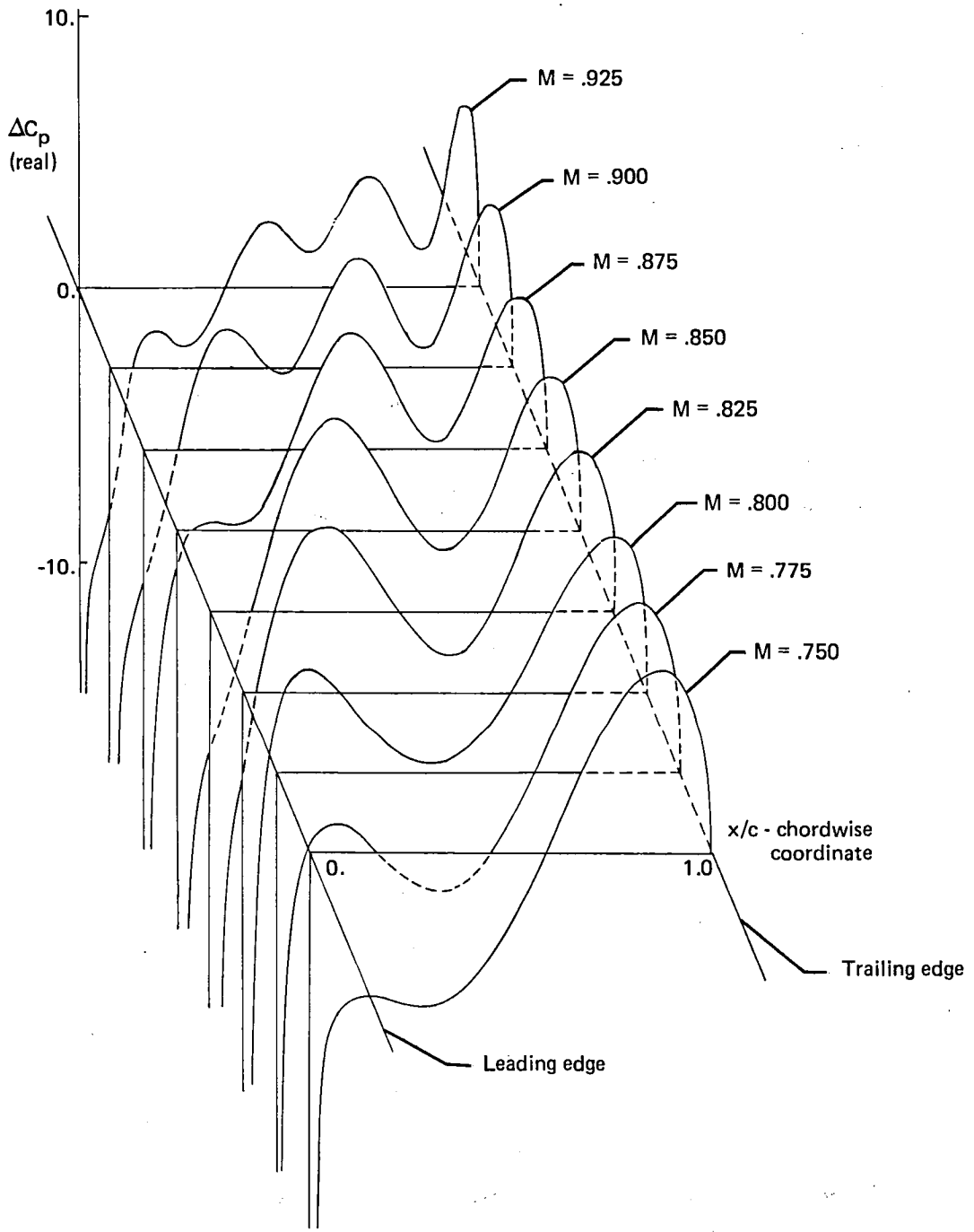

Figure 12.—Real Part of Pressure Coefficient Distribution at the Centerline of a Rectangular Wing Due to Airfoil Plunging as a Function of Mach Number with k = 1.0

A constant reduced frequency, k = 1.0 is maintained for all Mach number variations. The resulting converged pressure distributions become increasingly wavy with an increase in Mach number.

Figure 13 represents a plot of the number of chordwise pressure terms required for convergence in the various Mach number analysis cases of figure 12. This illustrates the need of using additional chordwise pressure modes in analyses using high Mach number and/or large k values.

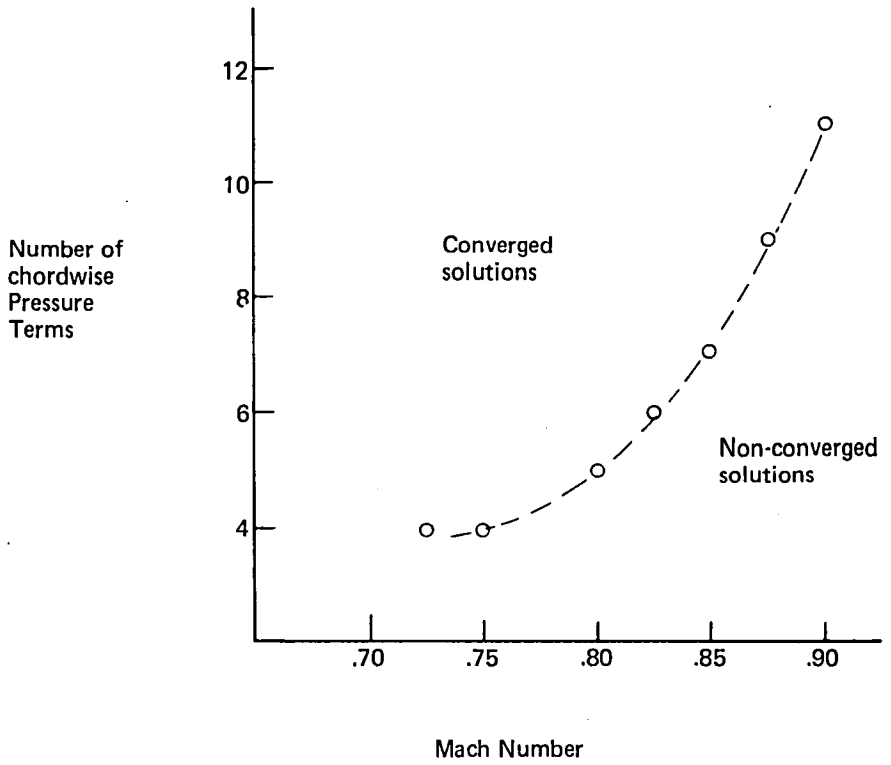

Figure 13.—Number of Chordwise Pressure Terms Required for Convergence as a Function of Mach Number with k = 1.0

Validation of the program accuracy in predicting unsteady loadings in analysis cases using high Mach number and/or large k values has been accomplished by comparing the results of this program with the results of other theoretical prediction methods. Centerline pressure distributions of a high aspect ratio wing planform obtained by the present program are compared with distributions obtained from a two-dimensional airloads program developed by NASA LRC. The pressure distributions should be identical in the limit as the aspect ratio becomes very large.

Figure 14 and figure 15 represent the real and imaginary parts of pressure coefficient distribution respectively. The continuous solid lines represent the predicted pressure coefficient distributions obtained from the two-dimensional program of NASA LRC and these distributions are used as a standard of reference. The circle symbols represent the predicted results of the present three-dimensional program that obtained pressure distributions near the centerline of a rectangular wing of aspect ratio 10 that is pitching about the leading edge at k = .9 with M = .9. The small differences existing between the results of the two prediction methods is thought to be due to approximating two-dimensional flows by the results of an analysis of a finite span wing using a three-dimensional prediction technique.

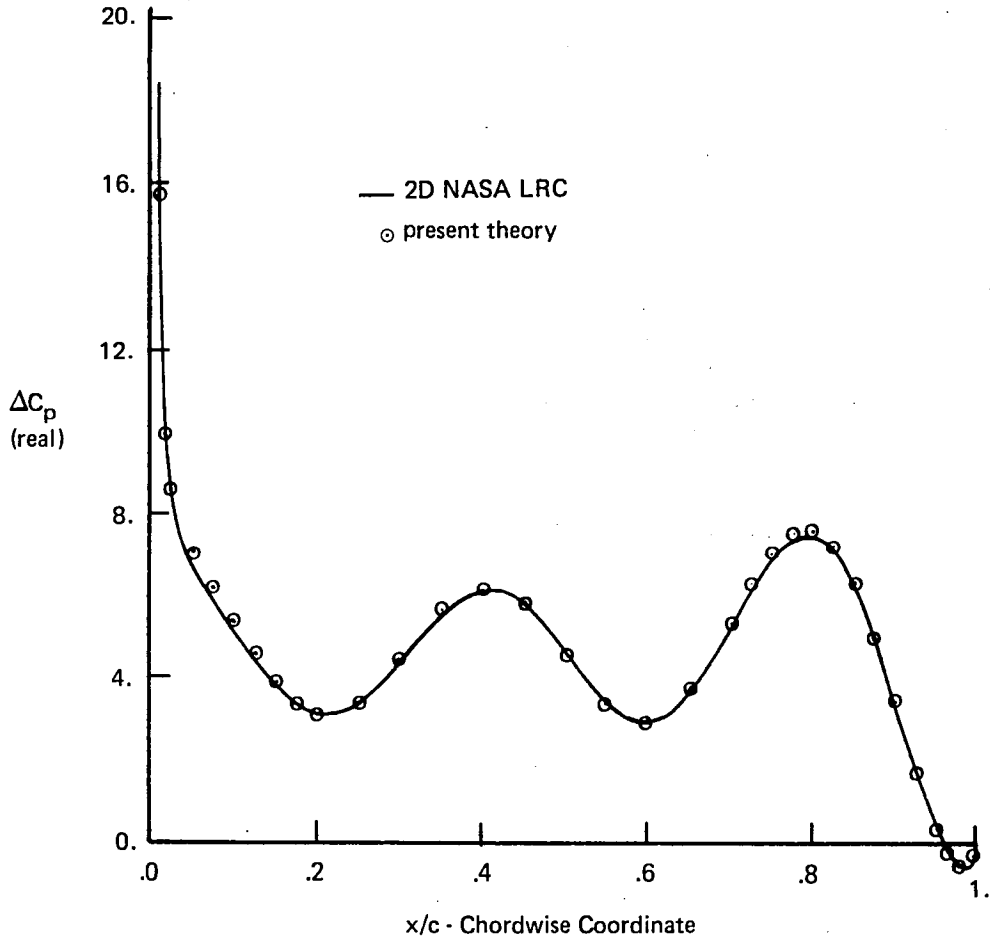

Figure 14.—Real Part of Pressure Coefficient Distribution Due to Airfoil Pitching About the Leading Edge at k = .9, M = .9

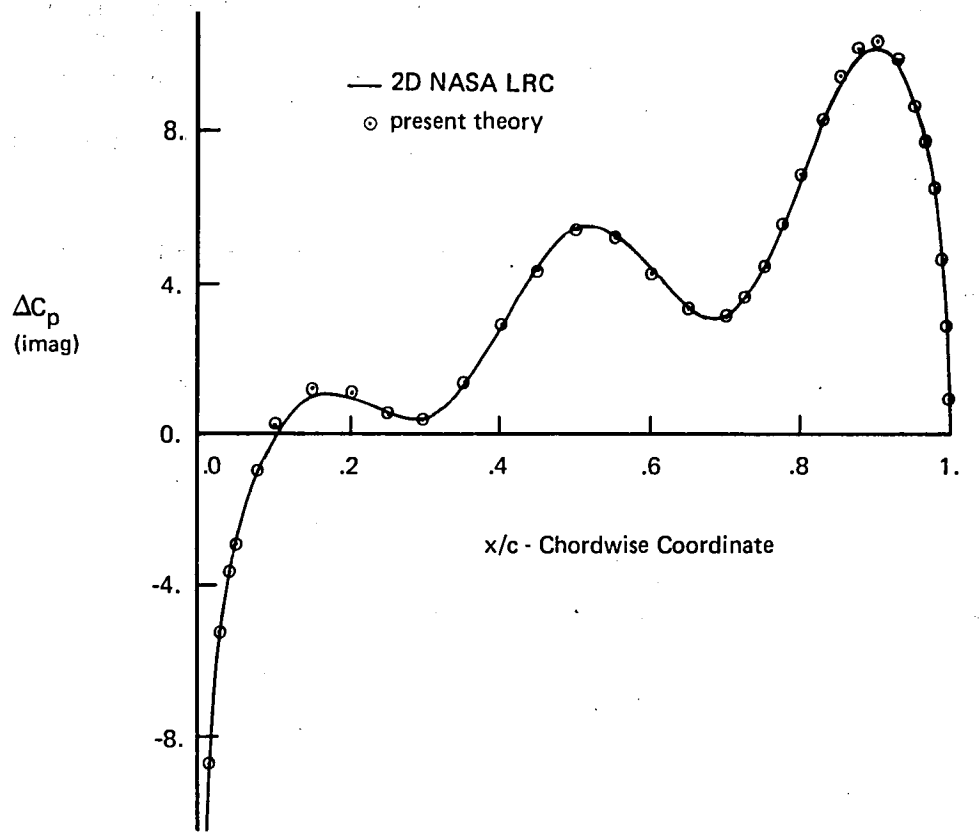

Figure 15.—Imaginary Part of Pressure Coefficient Distribution Due to Airfoil Pitching About the Leading Edge at k = .9, M = .9

Numerical investigations indicate that converged solutions may be achieved for high k value-Mach number conditions using the following equation to estimate largest k value for which converged solution may result for a given analysis Mach number.

$$k_{max} = \frac{(1 - M^2)}{M} (.4444444) (NDWPC)$$

where NDWPC is the number of downwash points per chord

Since the maximum number of chordwise downwash stations allowed by the program is 12, the user can then determine the highest k value (for a given M) for which valid solutions may be obtained by setting NDWPC = 12 in the above equation.

The above k value is referenced to the root semi-chord. If other reference lengths are used to define k then appropriate changes should be made in the above equation such that the proper upper limit of usable k value may be identified for which valid solutions may be obtained.

It should be noted the arbitrary selection of downwash stations per chord is eliminated by an actual determination of the minimum number of chordwise downwash stations required for a given Mach number - k value analysis. The minimum number may be established by plotting the generalized forces against the number of downwash stations per chord as indicated in figure 11 and selecting the smallest number of downwash stations that provide converged solutions for analyses that involve high Mach number, high k values, and camber bending mode shapes.

It is also recommended that a minimum of 4 downwash points per chord be used in analyses involving any camber bending mode shape.

INCREASED ACCURACY USING PLANFORM SMOOTHING

Practical planforms usually contain one or more spanwise stations where slope discontinuities exist in either the leading edge or trailing edge. A typical planform having slope discontinuities in its edge is shown in figure 16 which represents the planform of the Boeing 727 commercial transport.

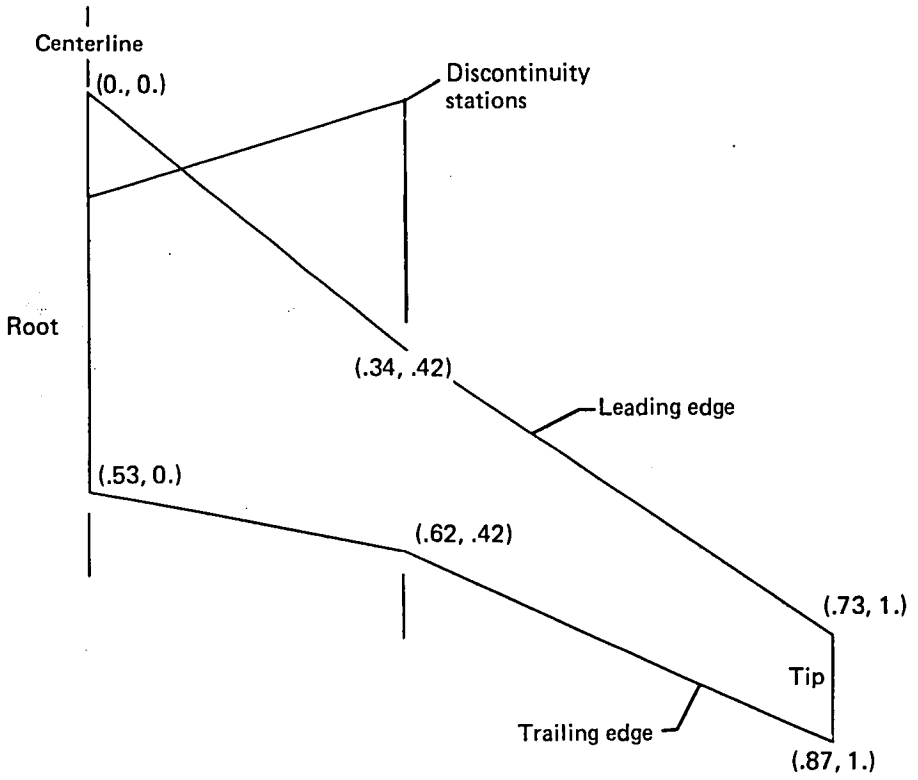

Paired numbers are non-dimensional planform coordinates

Figure 16.—Typical High Aspect Ratio Planform Having Slope Discontinuities in Leading Edge and/or Trailing Edge Definitions

Investigations indicate that theoretical unsteady loadings predicted for planforms having edge slope discontinuities are highly dependent on the location of downwash chords relative to the discontinuities. Figure 17 shows predicted spanwise loadings for the planform shown in figure 16, using three different downwash chord distributions. Each theoretical distribution exhibits a localized waviness that is inconsistent with experimental results.

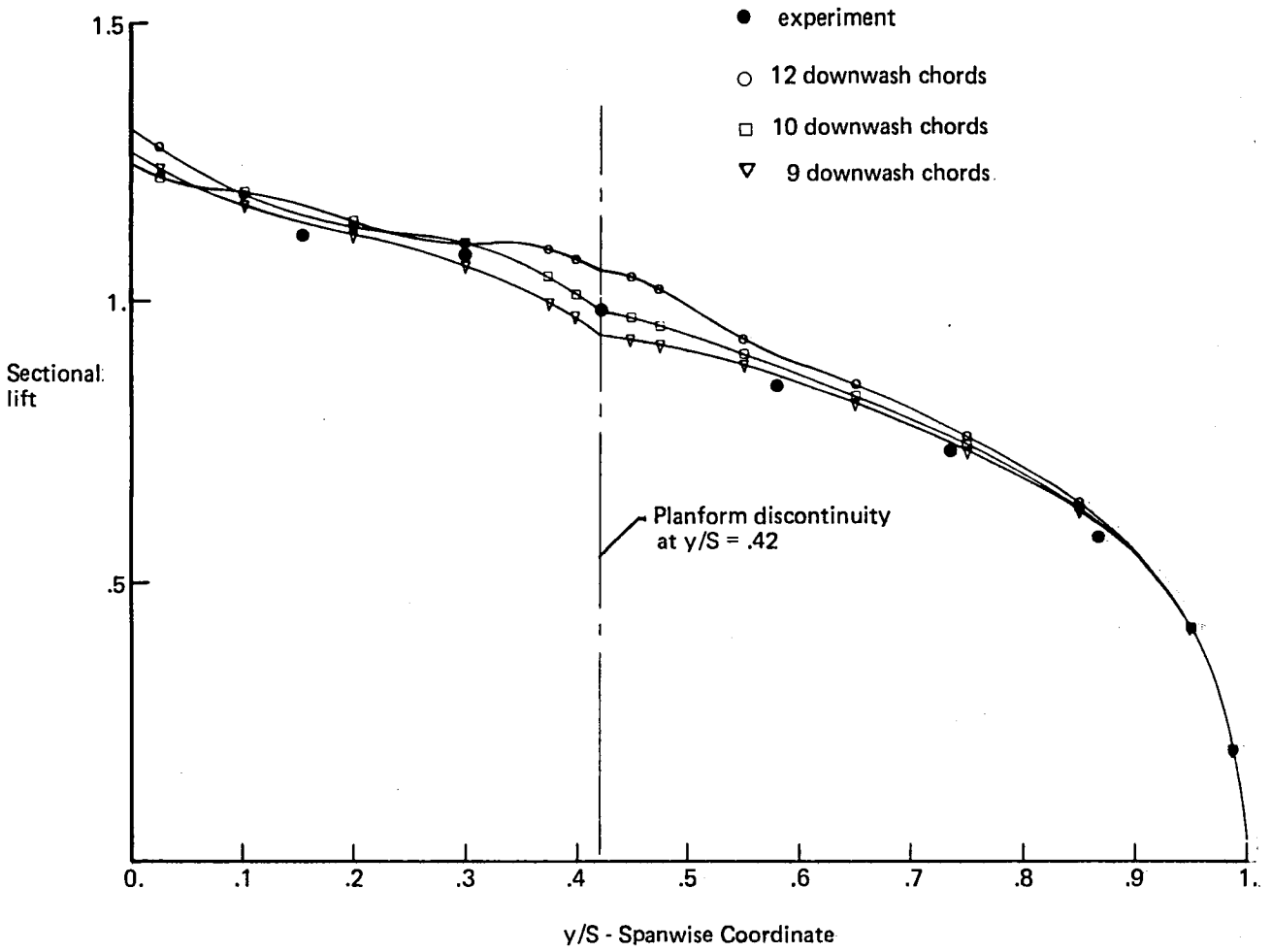

Figure 17.—Comparison of Theoretical and Experimental Spanwise Lift Distributions on the 727 Planform at M = .55, k = 0

The only difference in input data for the theoretical predictions is the number of downwash chords used in the individual analyses. Figure 18 shows the spanwise distribution of downwash chords applied in each analysis case.

The 12 downwash chord distribution contains one chord that is located very close to the spanwise discontinuity station. The predicted loadings resulting from this distribution deviate from the experimental results by the greatest amount in comparison with the other theoretical results.

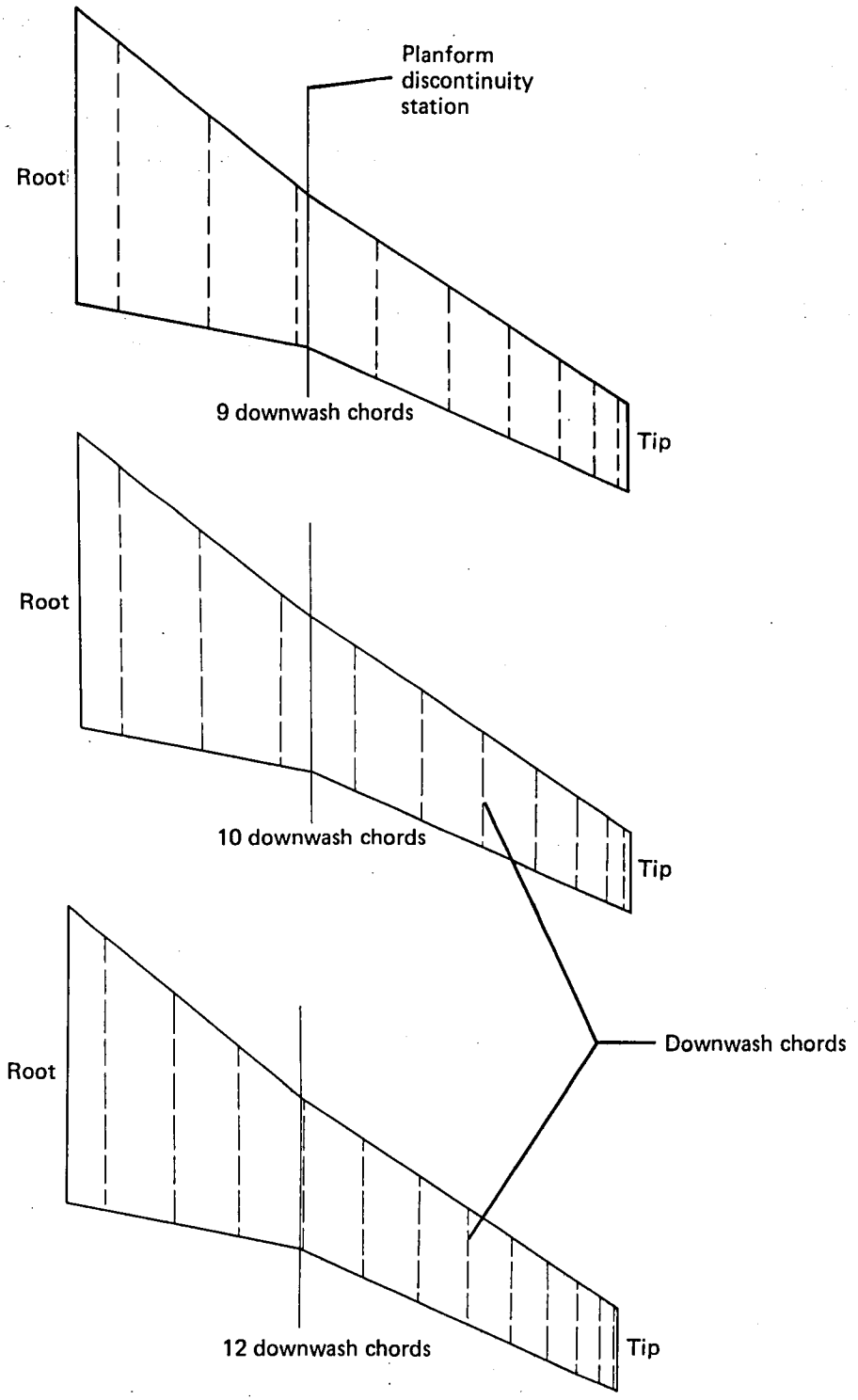

Figure 18.—Distribution of Downwash Chords Used in Analyses of 727 Planform

A numerical investigation has been conducted to identify the cause of the wavy spanwise loadings and lack of convergence with increasing number of analysis downwash chords.

The investigation concentrated on examining the characteristics of theoretical downwash sheets developed for planforms having slope discontinuities in leading and/or trailing edge definitions.

The analysis planform, used in the numerical investigations, shown in figure 19 has a slope discontinuity at the centerline for both the leading and trailing edges as well as having a trailing edge slope discontinuity at the 50 percent semispan station.

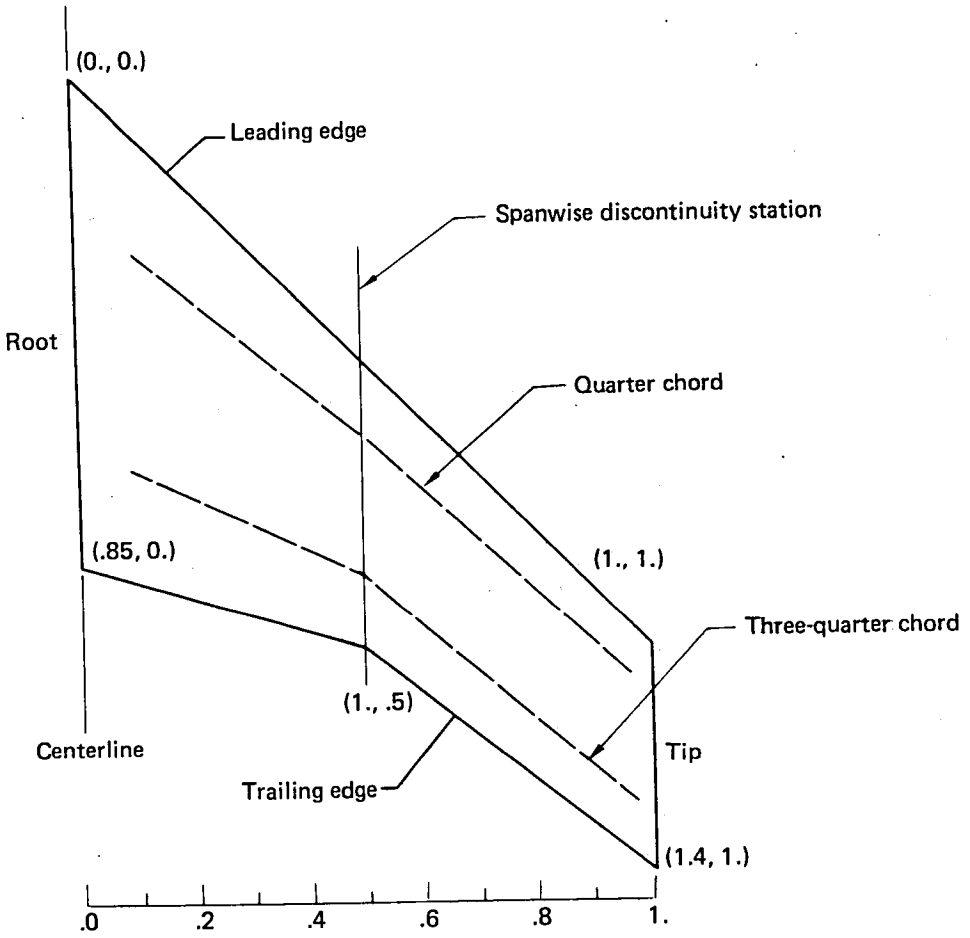

Figure 19.—Analysis Planform Used in Identifying the Cause of Wavy Spanwise Loadings

The downwashes (due to the first assumed pressure mode) calculated for stations along the quarter chord and the three-quarter chord stations are shown in figure 20 and figure 21 respectively. The downwashes become singular at spanwise slope discontinuity station and there is a larger variation along the three-quarter chord station than along the quarter chord station.

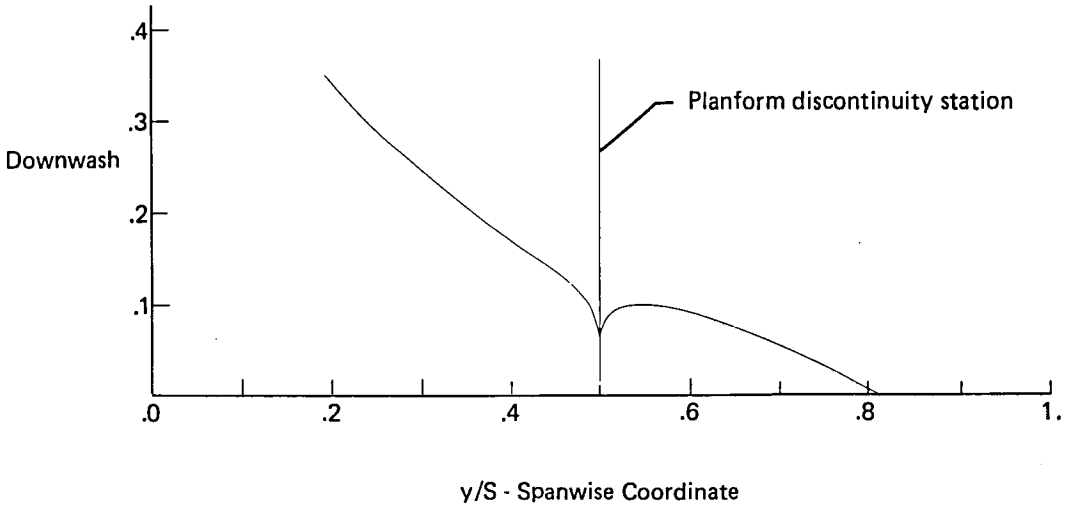

Figure 20.—Downwash Distribution Along the Quarter Chord Stations

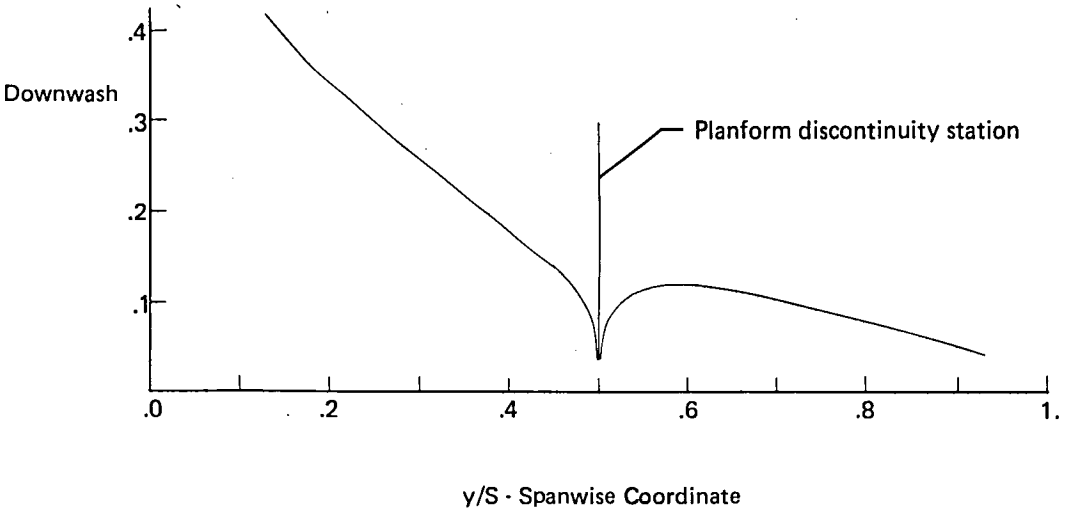

Figure 21.—Downwash Distribution Along the Three-Quarter Chord Stations

The next procedural step is one of examining the characteristics of the assumed pressure distributions along spanwise rays that crossed the slope discontinuity station as indicated in figure 21.

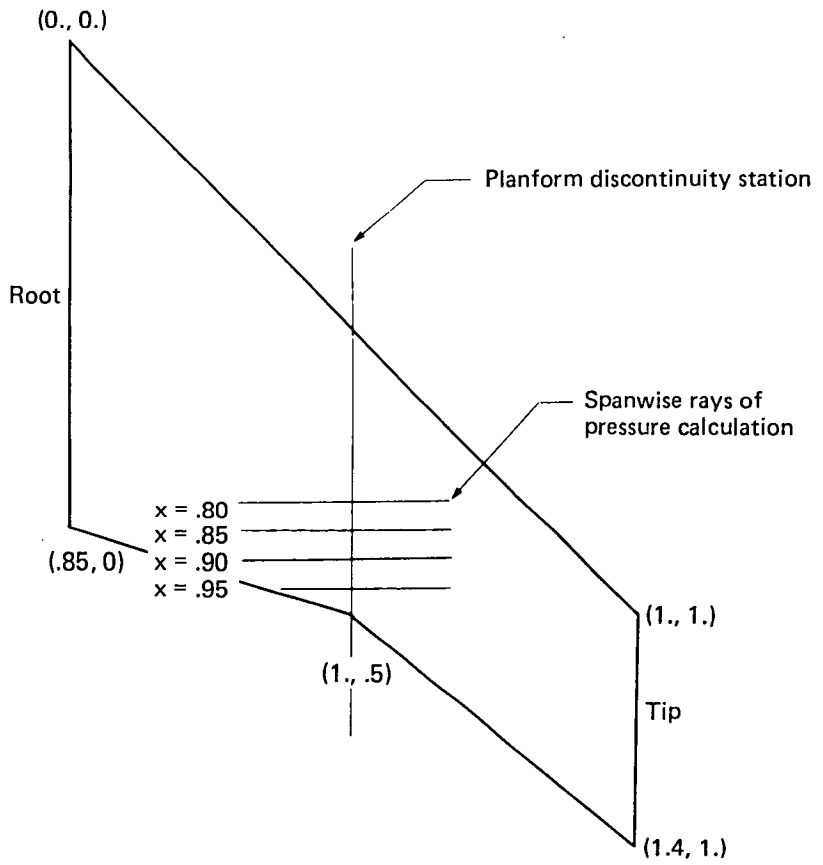

Figure 22.—Analysis Planform Showing Location of Spanwise Rays Where Surface Pressures are Calculated

Surface pressures (due to the first assumed mode) evaluated along spanwise rays of figure 22 are shown in figure 23. The spanwise pressures display slope discontinuities that increase in value towards the trailing edge. A basic requirement that must be satisfied for successful application of lifting surface theory is that the assumed pressure distributions must be analytically continuous through the second derivative in the spanwise direction. The assumption of having analytic continuity is satisfied for planforms having continuous derivatives in planform edge definitions. However, the assumption is not satisfied for planforms having slope discontinuities in edge definitions.

The singular downwash distribution (figure 21) is caused by the dipole term of the kernel function that produces downwashes that tend to become infinite if the spanwise loading functions do not exhibit second derivative continuity in the spanwise direction.

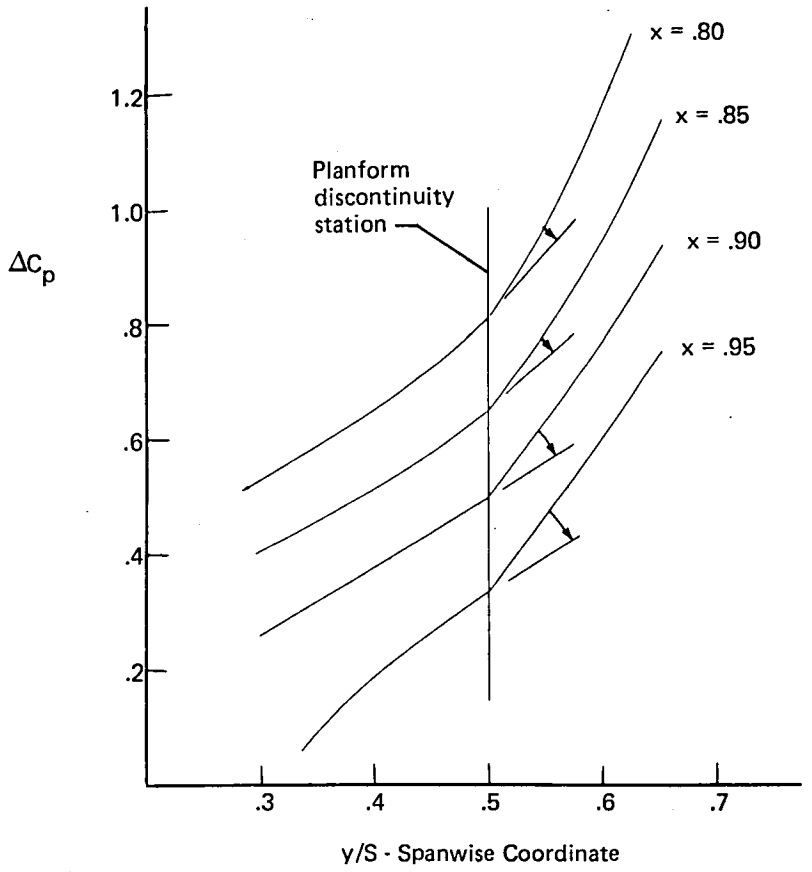

Figure 23.—Spanwise Pressure Variation Across Planform Discontinuity

A program option has been developed to provide second derivative continuity in the spanwise loadings to ensure converged solution results in analyses of planforms having slope discontinuities.

The technique is one of smoothing or redefining the planform edges by passing a chain of cubics (or a single cubic in the discontinuity region) through a set of planform stations that *do not* include the spanwise slope discontinuity station such as indicated by the circle symbols of figure 24. A maximum of 10 stations may be used to redefine the planform edges if the cubic chain option is activated.

It should be noted that the redefined planform definition is used throughout all subsequent calculations including pressure and generalized force calculations.

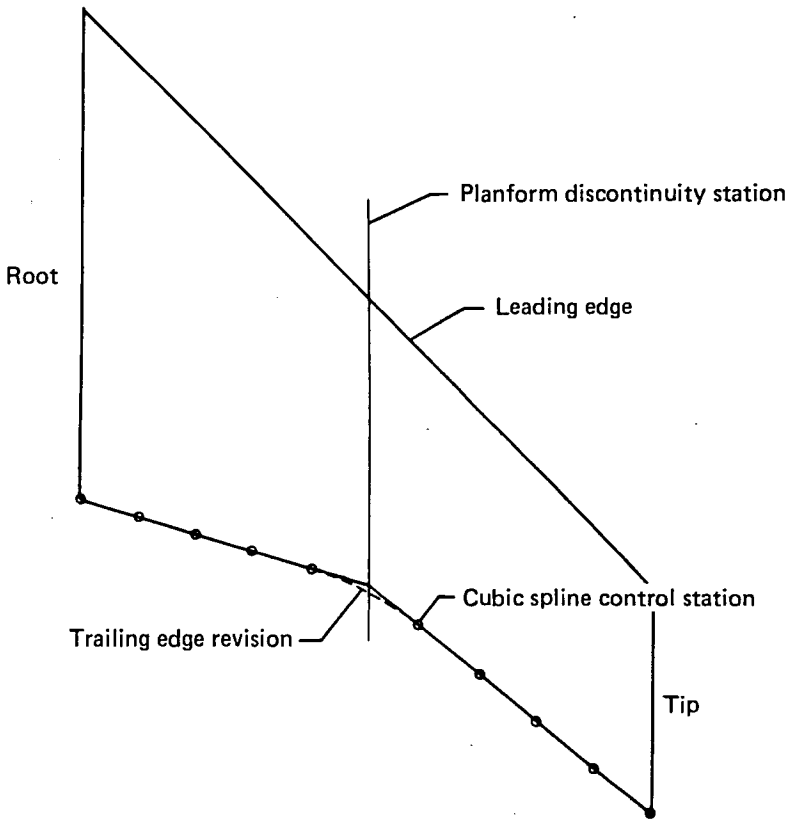

Figure 24.—Trailing Edge Revision Using Cubic Spline Smoothing Option

The planform definition using the cubic chain option differs only by a very small amount from the original planform definition for the regions outboard (and inboard) of the new definition station located on either side of the slope discontinuity station. For the region next to the slope discontinuity station, the cubic chain planform differed from the original planform (of this example case) as shown by the dashed line in figure 24. The amount of additional area added to the original planform area depends on the distance that the first cubic chain station (on either side of the discontinuity station) is located relative to the discontinuity station.

Figure 25 and figure 26 represent a comparison of downwashes generated along the quarter chord and three-quarter chord stations (figure 19) respectively for the original and the 10 point cubic faired planforms. The new downwash distribution of the cubic faired planform is continuous and does not cause any large local variations in the calculated downwash sheets if a downwash chord is inadvertently located near the original slope discontinuity station.

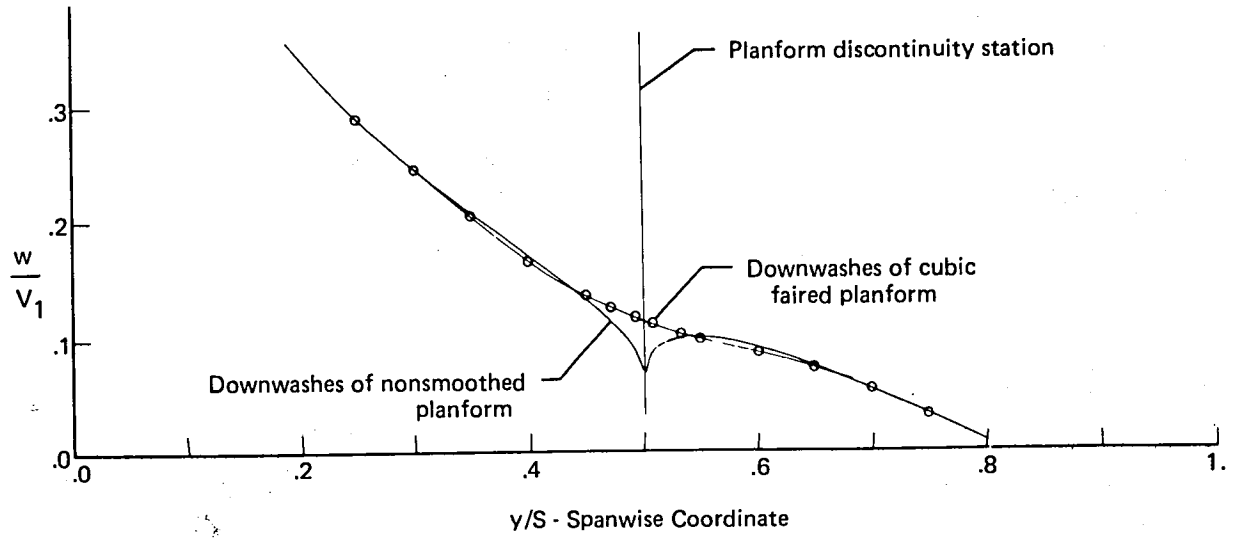

Figure 25.—Comparison of Downwashes Generated Along the One-Quarter Chord Line for Smoothed and Nonsmoothed Planforms

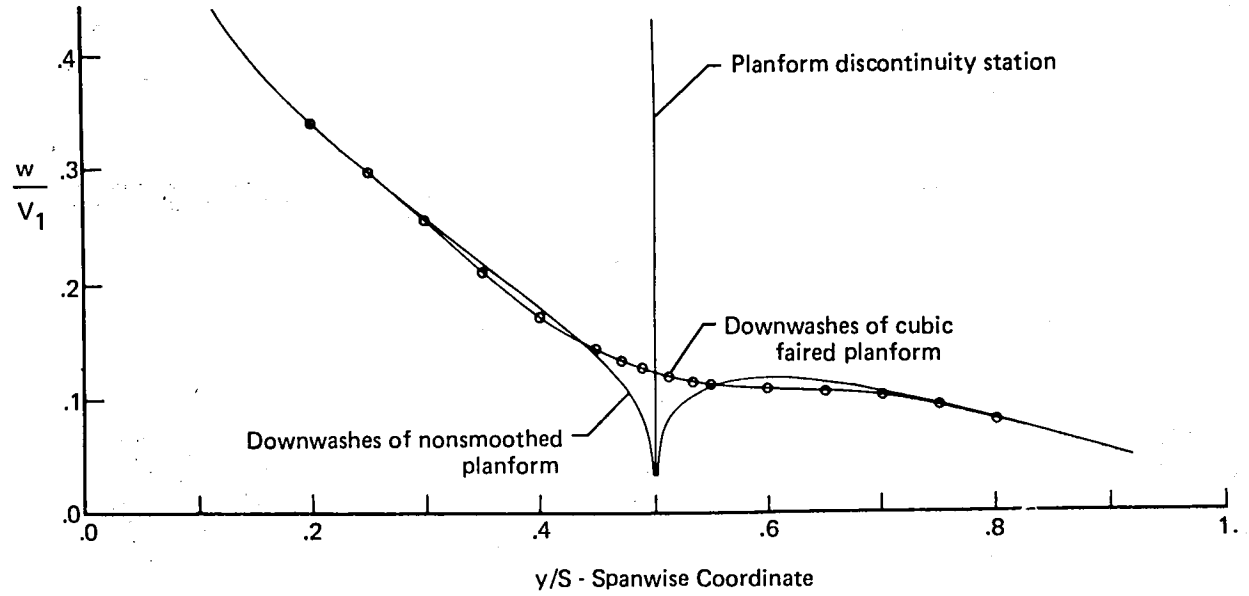

Figure 26.—Comparison of Downwashes Generated Along the Three-Quarter Chord Line for Smoothed and Nonsmoothed Planforms

The planform smoothing option was then applied in the analysis of the 727 wing of figure 16 and the analysis results are shown in figure 27.

The spanwise loadings predicted for the three downwash chord distributions appear to be almost identical and the theoretical results compare favorably with experimental results for each of the downwash chord analyses.

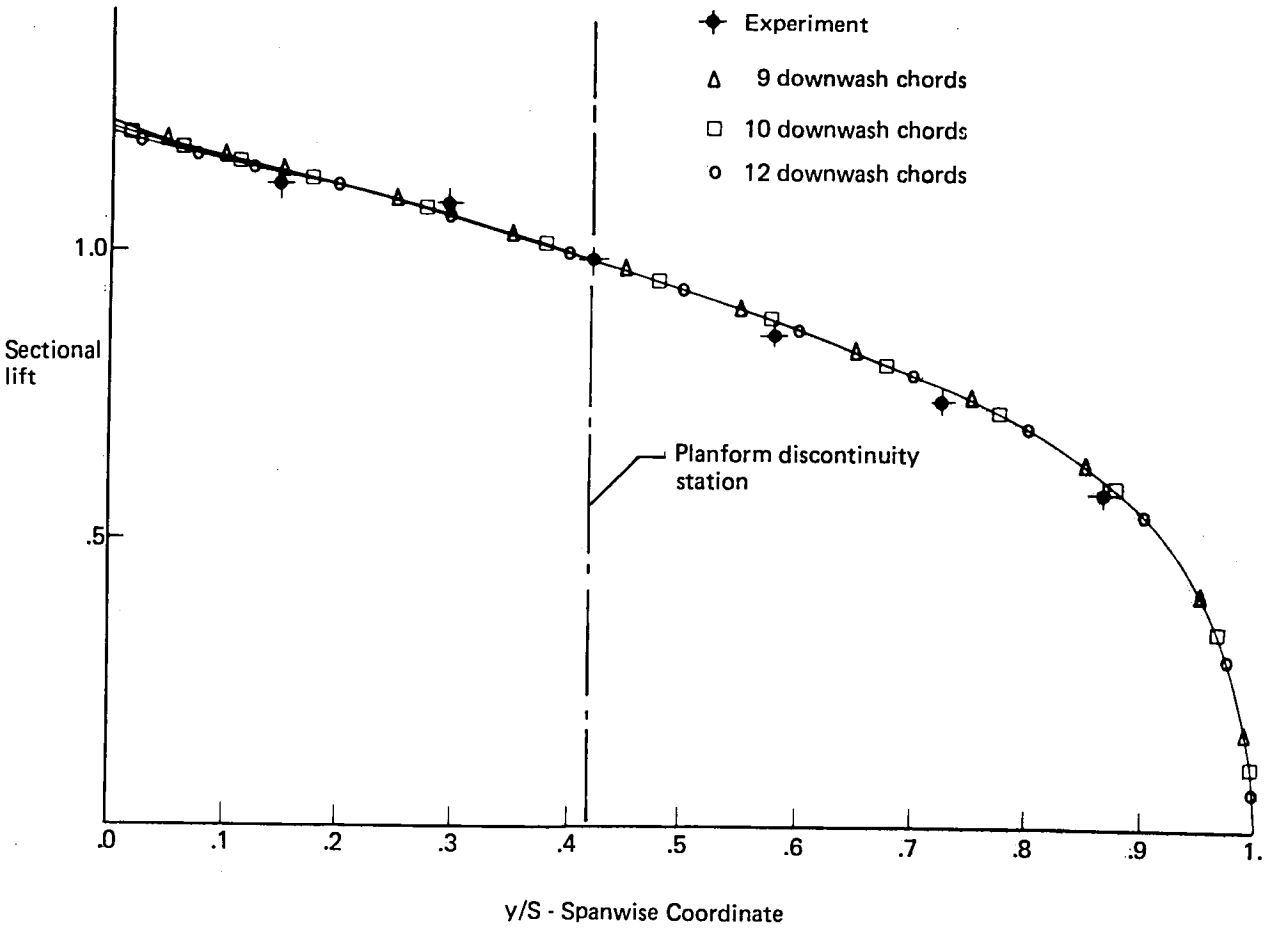

Figure 27.—Comparison of Experimental and Theoretical Spanwise Lift Distributions on the 727 Planform for M = .55, k = 0

Application of the planform smoothing option appears to result in converged solutions but at a cost of a minor change in planform geometry. Numerical investigations indicate that reasonably accurate solutions are obtained provided that the redefined planform stations on either side of the discontinuity station are located no closer than 5 percent of the semispan from the discontinuity station.

Two techniques are available for smoothing slope discontinuities. The first method consists of passing a chain of cubics over the entire length of a leading or trailing edge as described above. The second method is to locally modify the edge definition at the discontinuity station only and let the rest of the edge be defined by straight line segments. The following section describes the use of the cubic spline and the localized smoothing options and indicates modifications to be made in the RHOIV program document, NASA CR-145354, section 3.7.3.

The cubic spline option may be used to smooth either or both the leading and trailing edge. If selected, this option assures second derivative continuity everywhere, including the center line if desired, but results in a slightly reshaped planform that does not necessarily pass through the original definition points. To invoke this option, apply the following procedure:

1) if a leading edge spline is desired, specify SLE = .TRUE. on the RHOA namelist input record (default is SLE = .FALSE.);

2) if a trailing edge spline is desired, specify STE = .TRUE. on the RHOA namelist input record (default is STE = .FALSE.);

3) if the spline edge definition is applied, it is good practice to introduce additional edge definition points, spaced equally between break points - this practice will result in a planform closely resembling the original planform definition.

The localized smoothing option allows the user to select the points where smoothing is desired, along with the effective smoothing length. For each point to be smoothed, the planform is unchanged except within the vicinity of the break station at y. New definition points at y - d and y + d replace the point at y. The coefficients of the smoothing spline between are computed. The resulting planform definition has second derivative continuity everywhere, except for any break points not smoothed. To exercise the smoothing option apply the following:

1) if any leading edge definition points are to be smoothed, specify CLE = n on the RHOA namelist input record, where n = number of points to be smoothed (default is CLE = 0);

2) if any trailing edge definition points are to be smoothed, specify CTE = n on the RHOA namelist input record, where n = number of points to be smoothed (default is CTE = 0);

3) Leading and trailing edge definition points, card sets 2B and 2C, respectively, do not need to be changed at all.

4) Immediately following the trailing edge definition (card set 2C) insert:

   a) CLE pairs of values of the form (y,d) in 6F10.0 format, where each y is a break point station (ascending order) and d is the smoothing length.

   b) CTE pairs of values of the form (y,d) in 6F10.0 format, where each y is a break point station (ascending order) and d is the smoothing length.

Take special note of the following items:

1) The smoothing zone (y - d, y + d) of any break point should not overlap the zone of any other break point or include any other definition point.

2) The spline and localized smoothing options are incompatible. For example, a leading edge spline cannot be used if localized smoothing is done on the trailing edge.

3) Localized smoothing can be applied at the center line, if desired.

MODIFICATION OF DOWNWASH CHORD DISTRIBUTION

Accurate predictions of unsteady loadings are obtained for conventional wing-control surface configurations using the program generated downwash chord distributions that are described as being a Gaussian distribution. However, unusual configurations may be difficult to model (within the program limitations) due to some unusual configuration characteristic. It is possible that the limited number of Gaussian downwash chord distributions (available in the program) may not allow a sufficient number of downwash chords for accurate load predictions due to a wavy residual downwash distribution.

For example, consider the wing-control surface configuration shown in figure 28 that has a very small span control surface located near the mid-span station of the wing. The residual

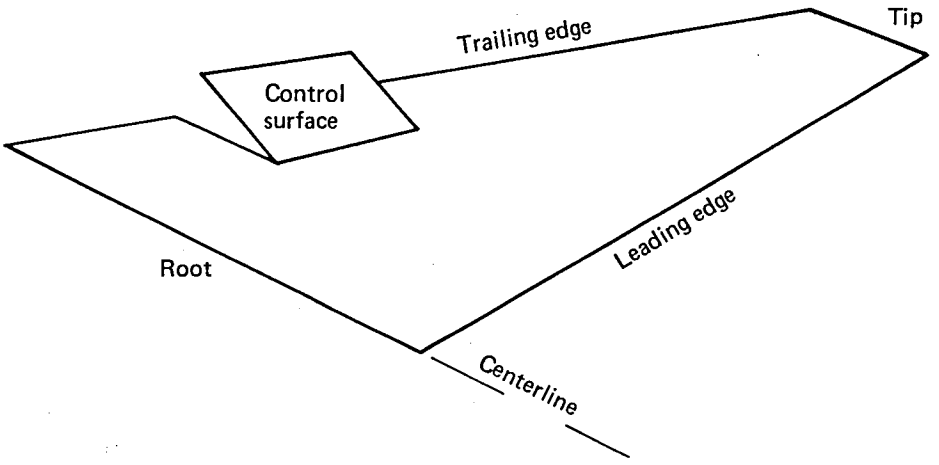

Figure 28.—High Aspect Ratio Planform With a Small Span Control Surface Located Near Planform Centerline

downwash distribution may have characteristics shown in figure 29. Waviness in the residual distribution is confined to the region containing the control surface and is relatively nonwavy over the rest of the planform. If it is suspected that the program Gaussian distributions may not provide a sufficient number of downwash chords located in the vicinity of the control surface to properly evaluate the local wavy residual distribution it may be desirable to use a downwash chord distribution different from that available in the program.

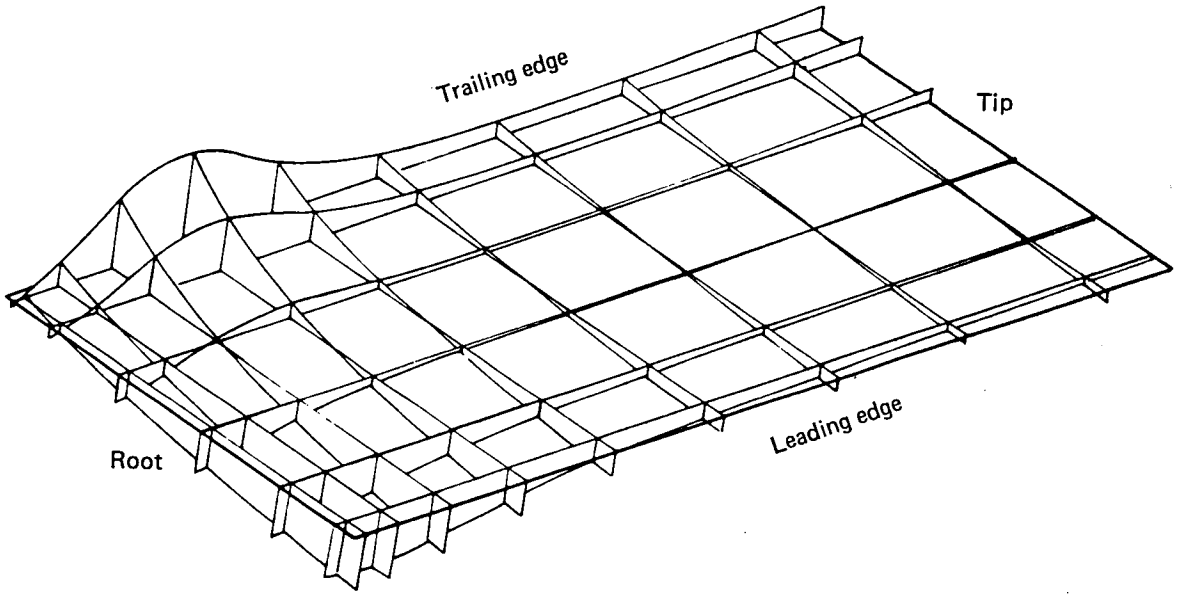

Figure 29.—Residual Downwash Distribution Due to Control Surface Deflection

Numerical investigations indicate that accurate predictions of unsteady loadings may be obtained for downwash chord distributions that do not have an overall Gaussian characteristic. The Gaussian downwash chord distributions have been developed on the basis of minimum error in load predictions provided that the spanwise loadings approach zero in proportion to the square root of the distance from the tip. The numerical experiments indicate that accurate solutions may be obtained provided that the outboard region near the tip (outboard of the 75 percent semispan station) has a downwash chord distribution that is Gaussian and the inboard region have uniformly spaced downwash chords.

A program option is available for user input of a downwash chord distribution that may be more suitable for a particular analysis configuration than the Gaussian distributions available in the program.

A schematic of such a non-Gaussian downwash chord distribution that has been successfully applied in control surface analyses is shown in figure 30. The distribution of figure 30 represents just one of many such distributions that will provide accurate loading predictions.

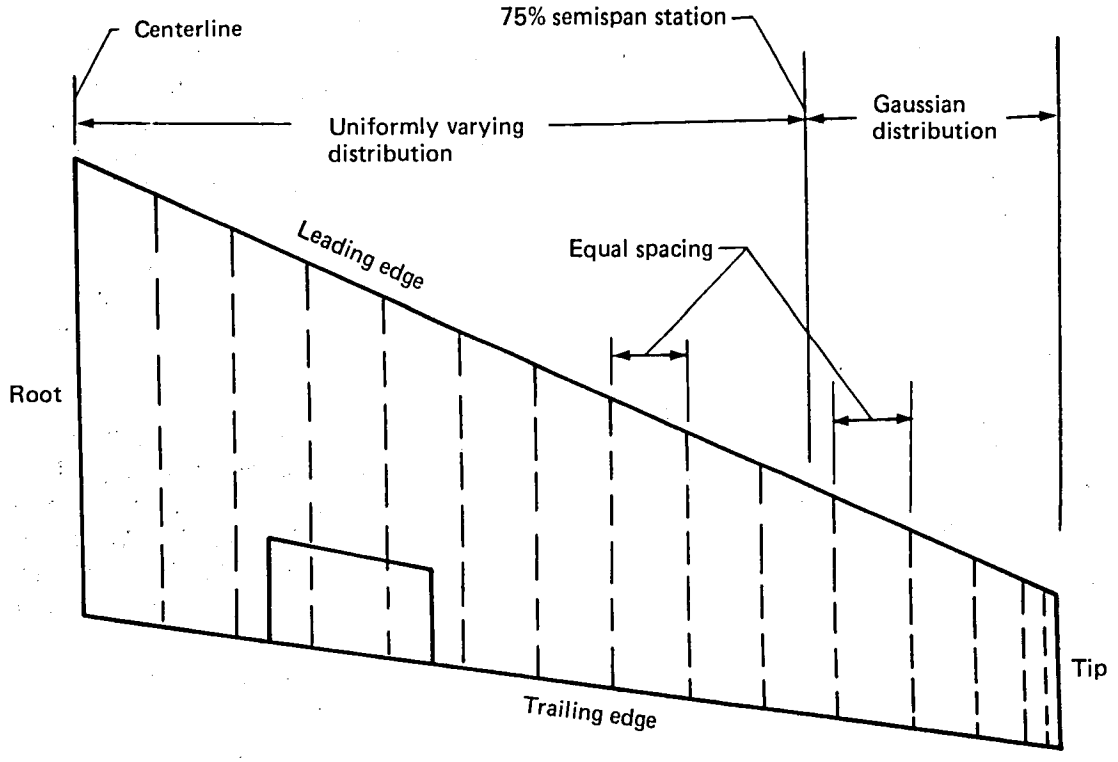

Figure 30.—Non-Gaussian Downwash Chord Distribution Used to Calculate Unsteady Loadings on a Small Span Inboard Control Surface Configuration

The downwash chord distribution outboard of the 75 percent semispan station contains the first five downwash stations defined for an eleven downwash chord Gaussian distribution. The downwash chord distribution inboard of the 75 percent station is an equally spaced distribution having a spacing equal to the spacing between the fourth and fifth chords of the Gaussian distribution. The only spacing requirement for the inboard region is that the spacing should vary uniformly without irregularities or large changes in spacing between any three consecutive downwash chords.

Consequently, the application of this user option allows greater flexibility in modeling unusual configurations with a downwash chord distribution that may be more suitable for a particular analysis configuration than that available with the Gaussian distribution contained in the present program.

RESULTS AND TIMING COMPARISONS

This section contains comparisons of theoretical and experimental data that result from analyses and tests of four wing-control surface configurations. The experimental configurations consist of: 1) a swept wing having a full span flap (reference 5); 2) a swept wing having a partial span control surface (reference 6); 3) a swept wing having oscillating side-by-side control surfaces (reference 4); 4) a highly swept delta wing having leading edge and trailing edge control surfaces (references 7 and 8).

Theoretical pressure distributions are provided for a subsonic transport-type wing and control surface configuration to demonstrate the use of higher order spanwise pressure terms in analyses of high aspect ratio wing-control surface configurations.

Computer timing results are provided for each of the above analysis cases. Computer usage costs (given in CP seconds) were obtained for the original program reported in NASA CR-2543 (reference 1) and also for the present prediction method. The results and timing comparisons are applicable for the extended verison of the program described herein. An estimation of the reduction in computer usage cost is obtained by comparing the CP seconds required for the two methods. All results were obtained in a CDC Cyber 175 computer having an FTN compiler with the optimization option set to 2.

STEADY-STATE RESULTS FOR FULL-SPAN FLAP CONFIGURATION

The full-span flap configuration of reference 5, for which measured pressures were obtained with various combinations of flap deflection and angle of attack, is shown in figure 31. The flap deflection and wing angle of attack were maintained at constant values for each experimental run.

Experimental pressures were obtained along a streamwise section located at the 50% semispan station. The longitudinal junction between wing and flap was sealed to prevent leakage between the lower and upper surfaces at the hinge line.

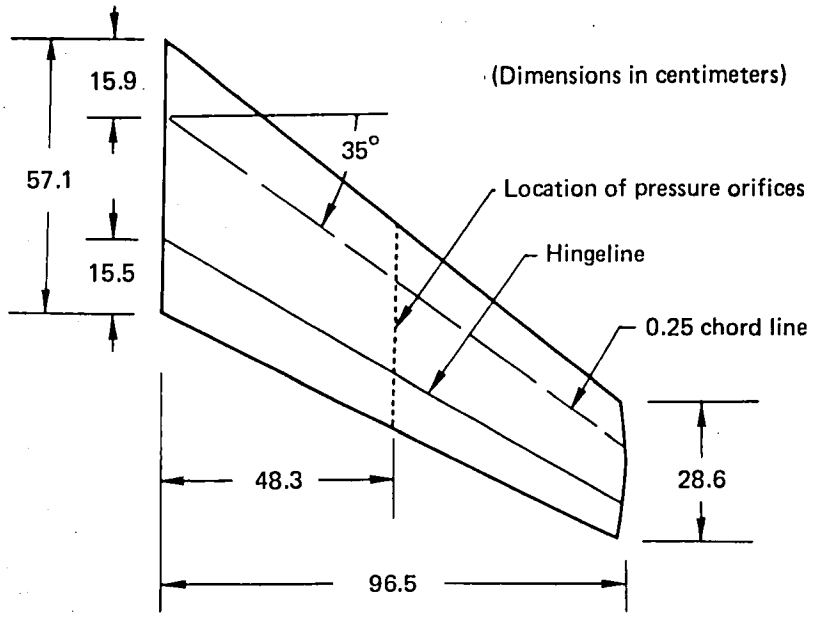

Figure 31.—Experimental Full-Span Flap Configuration of NACA RM A9G13

The theoretical pressure distributions were obtained for modified boundary conditions that account for local streamwise velocity variations due to airfoil thickness effects. A comparison of the experimental and theoretical results is shown in figure 32.

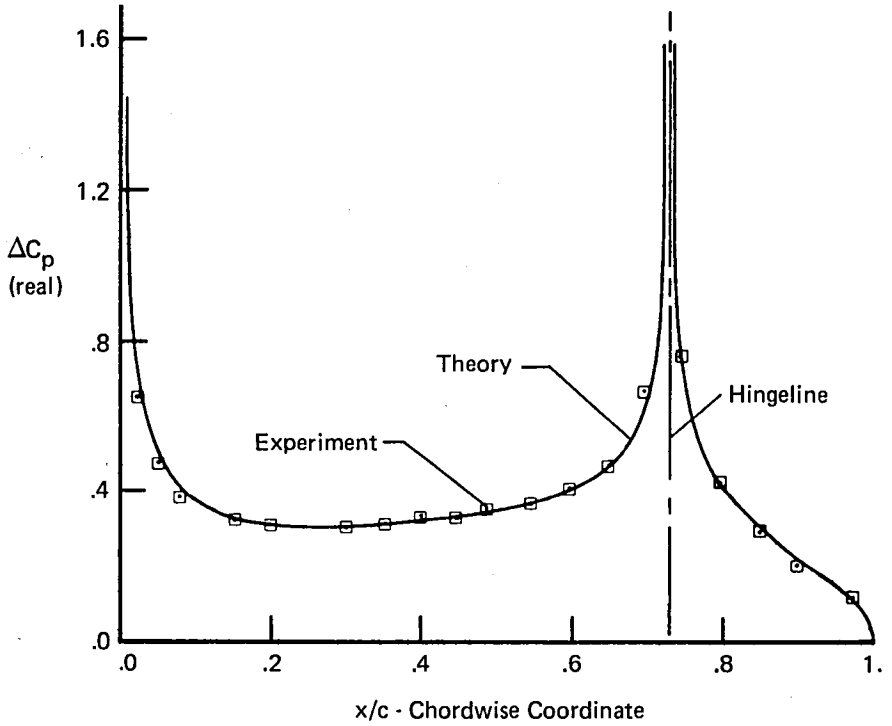

Figure 32.—Theoretical and Experimental Chordwise Pressure Distribution Obtained for a Full-Span Flap with $\delta = 10°$, $\alpha = 0°$, $M = 0.21$, $k = 0$

Since the sealed gap condition at the hinge line satisfies the theoretical assumptions (reference 3) a suitable basis is provided for evaluating the accuracy of the theoretical prediction. This comparison indicates that the experimental values are theoretically predicted within very close tolerances over the entire length of the chord, even in the vicinity of the hinge line.

Timing comparisons are shown in table 1 for two Mach number conditions. The results indicate that there is a small increase in relative computer costs with increasing Mach number.

Table 1.—Computer Timing Results for Steady-State Analysis of Full-Span Control Surface Configuration

			NASA CR-2543 (sec.)	NASA CR-3009 EXTENDED (sec.)	RATIO
	Total execution time		86.064	50.116	.582
M = .21	Main surface C-matrix	Total	5.842	2.797	.479
		Per DWP	.243	.117	
	Control surface C-matrix	Total	34.512	20.518	.594
		Per DWP	1.438	.855	
M = .80	Main surface C-matrix	Total	5.882	2.831	.481
		Per DWP	.246	.118	
	Control surface C-matrix	Total	34.513	20.709	.600
		Per DWP	1.438	.863	

STEADY-STATE RESULTS FOR A PARTIAL-SPAN FLAP CONFIGURATION

The configuration with partial-span control surface, shown in figure 33, is taken from reference 6, representing a planform that was used in obtaining chordwise pressure distributions due to steady flap deflection. Pressures were obtained on a chordwise section located at the 46% semispan station. The hinge line gap was sealed, providing a suitable basis for comparing theoretical and experimental results.

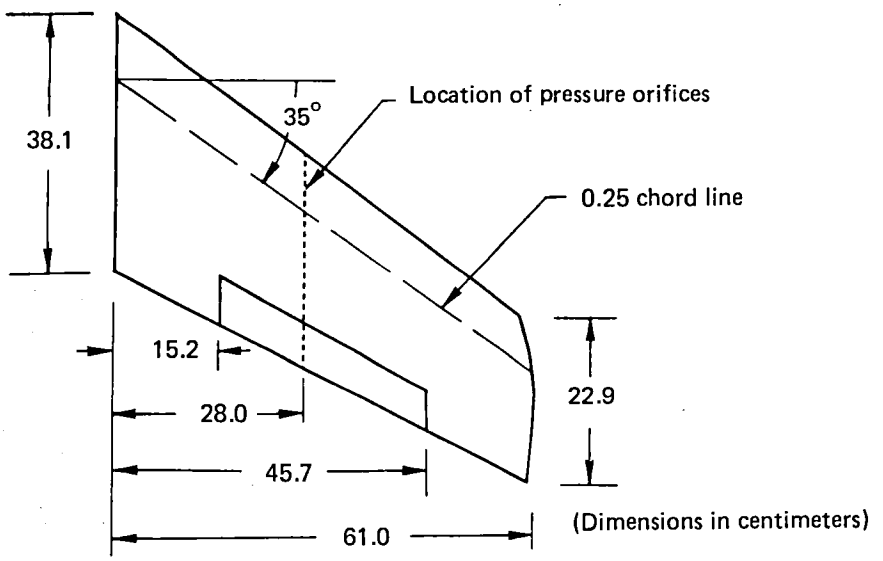

Figure 33.—Experimental Partial-Span Control Surface Configuration of NACA RM L53C23

The pressure comparison shown in figure 34 indicates that the experimental pressures are accurately predicted by the theoretical technique over a chordwise strip forward of the hinge line. The theoretical pressures on the control surface are only slightly larger than the experimental values.

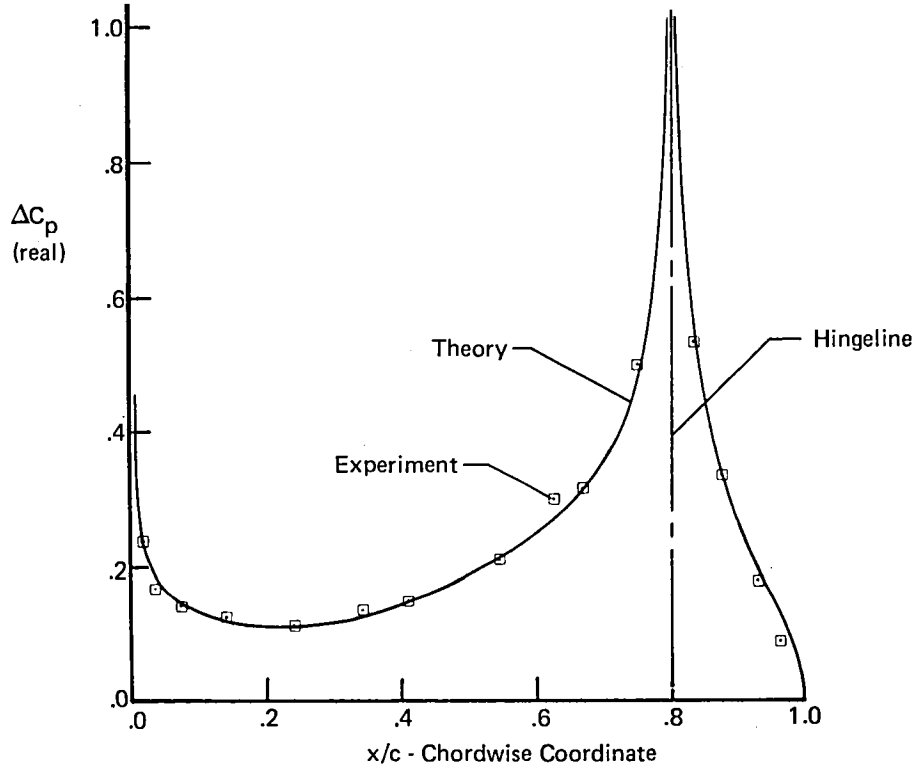

Figure 34.—Theoretical and Experimental Pressure Distribution for a Partial-Span Control Surface with $\delta = 10°$, $\alpha = 0$, $M = 0.60$, $k = 0$

Table 2 provides a measure of the computer costs involved for the two Mach number cases for both the original and revised prediction technique.

Table 2.—Computer Timing Results for Steady-State Analysis of Partial-Span Control Surface Configuration

			NASA CR-2543 (sec.)	NASA CR-3009 EXTENDED (sec.)	RATIO
	Total execution time		102.525	51.057	.498
M = .6	Main surface C-matrix	Total	9.071	4.787	.528
		Per DWP	.259	.137	
	Control surface C-matrix	Total	38.337	18.490	.482
		Per DWP	1.095	.528	
M = .8	Main surface C-matrix	Total	8.978	4.917	.548
		Per DWP	.257	.140	
	Control surface C-matrix	Total	37.935	19.049	.502
		Per DWP	1.084	.544	

SIDE-BY-SIDE CONTROL SURFACE CONFIGURATION

The side-by-side control surface configuration shown in figure 35 was used to obtain unsteady pressures for various combinations of flap deflections. The model has small open gaps at the hinge lines and side edges. Reference 4 provides no information on exact distances between control surface side edges and adjacent pressure measuring stations. The spanwise locations of experimental pressure chords were determined by measurement from the planform drawing.

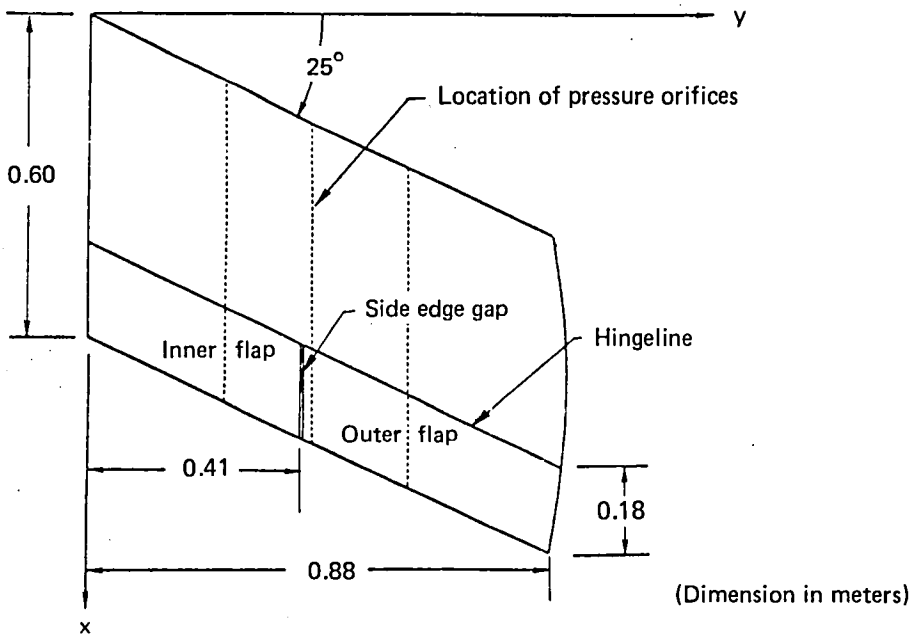

Figure 35.—Side-by-Side Control Surface Configuration

Figures 36 and 37 present comparisons of theoretical and experimental pressures along a chord located near the midspan of the oscillating control surface.

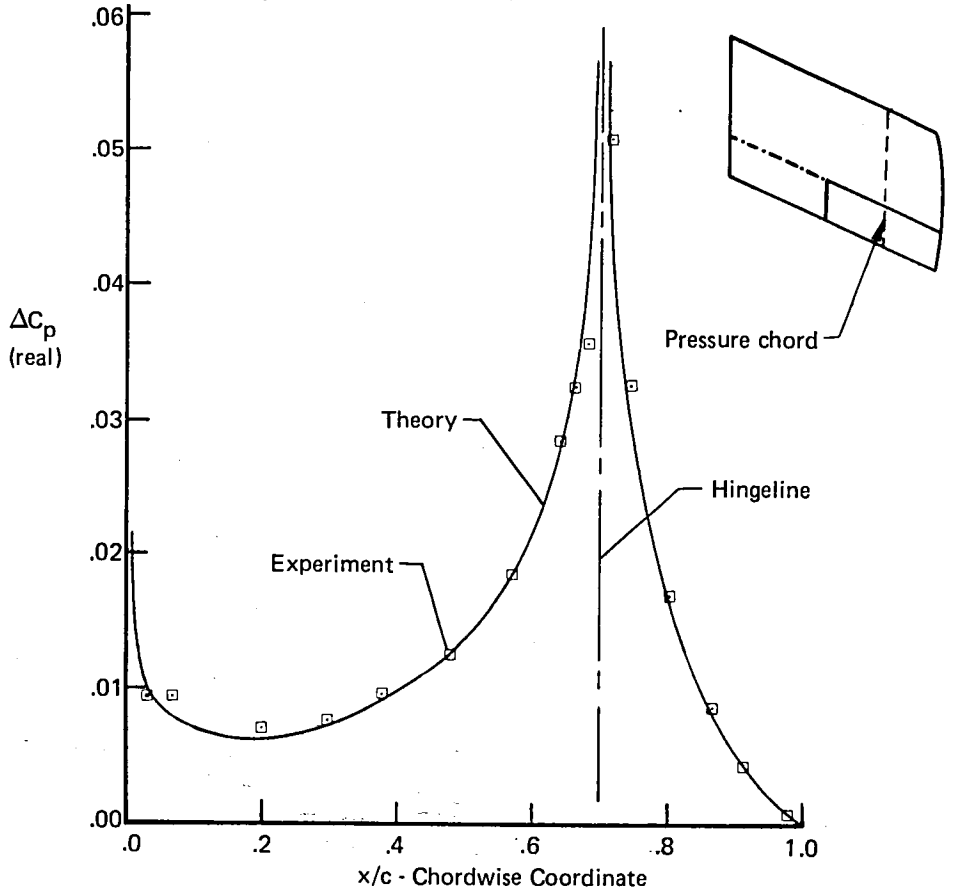

Figure 36.—In-Phase Part of the Chordwise Pressures Due to Motions of Outer Flap for a Pressure Chord Located on the Control Surface, M = 0, k = .372

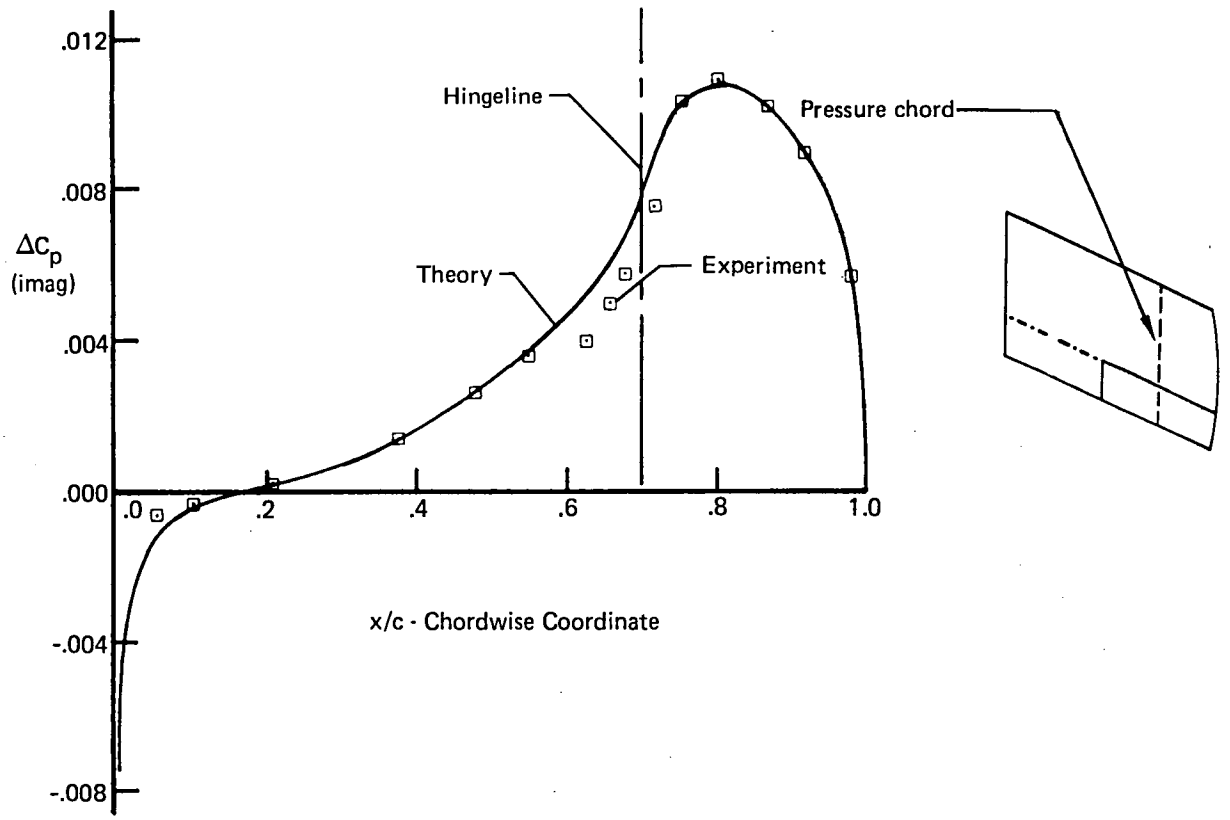

Figure 37.—Out-of-Phase Part of the Chordwise Pressures Due to Motions of Outer Flap for a Pressure Chord Located on the Control Surface, M = 0, k = .372

Table 3 presents timing comparisons to indicate relative computer costs for a six downwash chord analysis of the side-by-side configuration.

Table 3.—Computer Timing Results Obtained in Analysis of the Side-by-Side Control Surface Configuration

			NASA CR-2543 (sec.)	NASA CR-3009 EXTENDED (sec.)	RATIO
	Total execution time		218.284	60.283	.276
6 Downwash chords, 5 Points per chord	Main surface C-matrix	Total	17.481	7.672	.439
		Per DWP	.583	.256	
	Inboard flap C-matrix	Total	87.534	21.091	.241
		Per DWP	2.918	.703	
	Outboard flap C-matrix	Total	107.152	29.494	.275
		Per DWP	3.572	.983	

SWEPT DELTA WING WITH LEADING AND TRAILING EDGE CONTROLS

The configuration shown in figure 38 is taken from reference 7, wherein experimental studies were reported on the use of active controls to suppress flutter. Steady state hinge moments obtained in this investigation were published in reference 8.

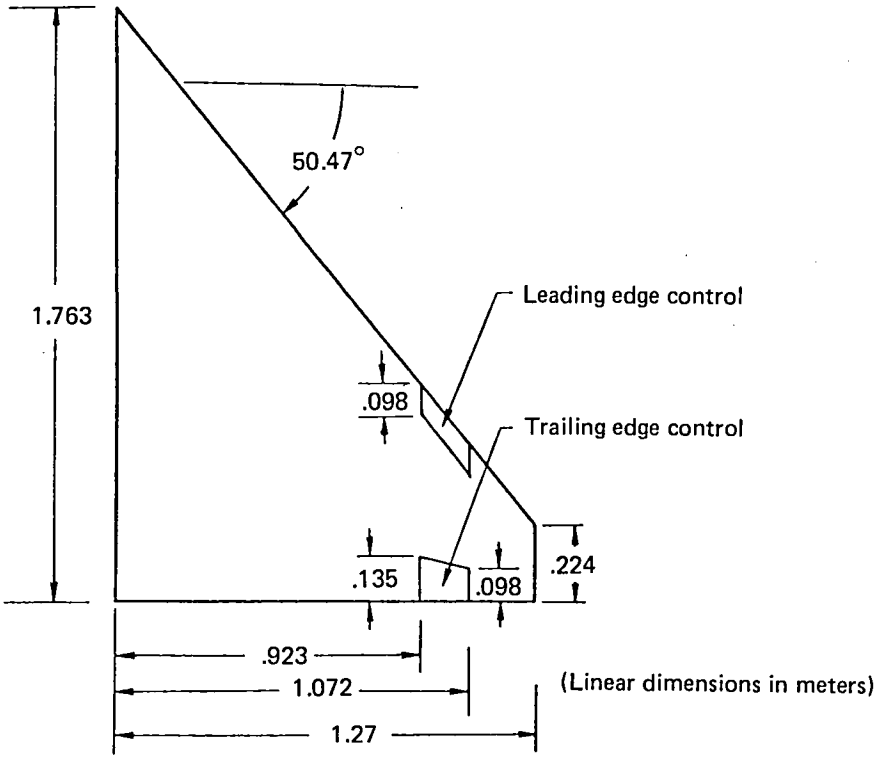

Figure 38.—Experimental Delta Wing Configuration of NASA TM X-2909

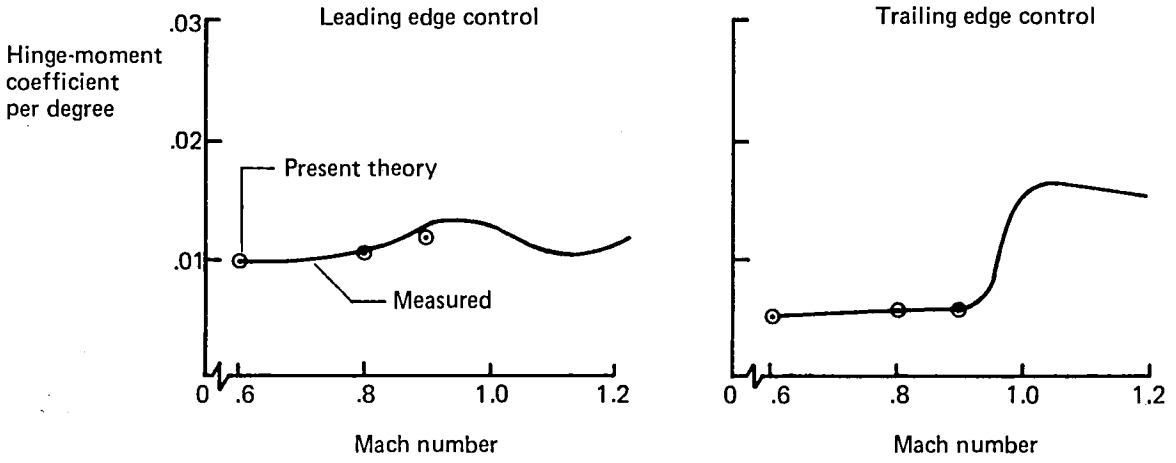

Figure 39.—Theoretical and Experimental Hinge-Moment Coefficients Obtained for Leading Edge and Trailing Edge Control Surfaces in Steady Flow

Figure 39 provides a comparison between theoretical and experimental hinge moments obtained for a leading edge and a trailing edge control surface deflection in steady flow.

Table 4 provides a relative measure of the cost reductions that may now be achieved for predicting unsteady loadings caused by motions of leading edge control surfaces.

Table 4.—Computer Usage Timing Comparisons Obtained for an Oscillating Leading Edge Control Surface at M = .8, k = .5

		NASA CR-2543 (sec.)	NASA CR-3009 EXTENDED (sec.)	RATIO
Total execution time		777.161	119.956	.154
Leading edge control surface C-matrix	Total	495.574	50.468	.102
	Per DWP	7.866	.801	
Trailing edge control surface C-matrix	Total	228.373	36.022	.158
	Per DWP	3.625	.572	
Main surface C-matrix	Total	43.182	27.270	.632
	Per DWP	.685	.433	

HIGH ASPECT RATIO TRANSPORT WING WITH CONTROLS

It should be noted that reasonable correlations obtained for the previous sample cases were achieved for configurations having large span control surfaces oscillating at small reduced frequencies. Numerical investigations conducted to evaluate solution convergence for small span control surfaces oscillating at high k values indicate that the number of analysis downwash chords needs to be increased in proportion to the k value and inversely proportional to the span length of the control surface.

Numerical investigations conducted to evaluate sensitivity in analysis of small span length control surfaces were accomplished using the wing and control surfaces configuration shown in figure 40. The 0.20 chord aileron has a length of 0.22 semispan and the 0.06 chord tab has a length of 0.12 semispan.

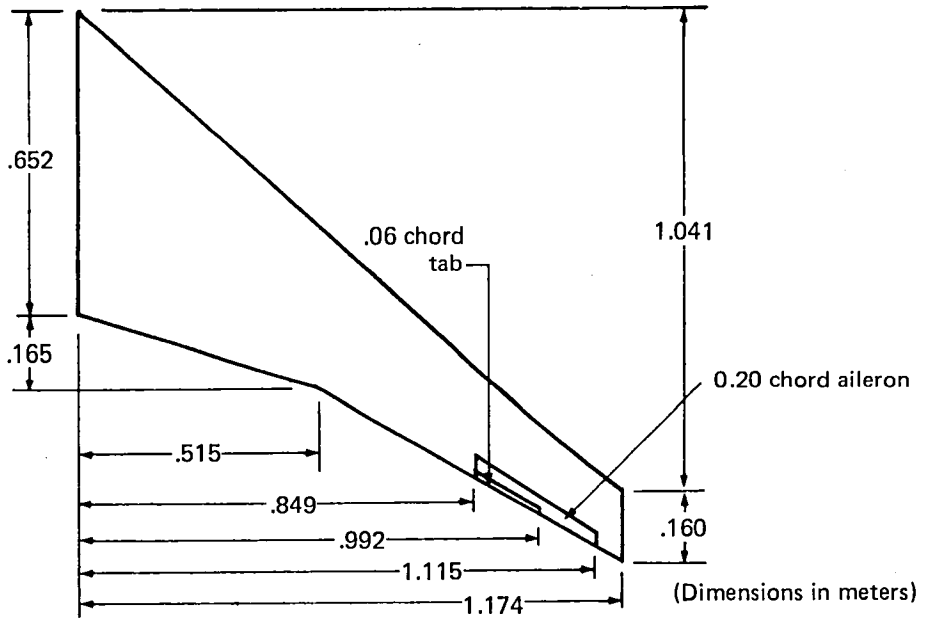

Figure 40.—Analysis Configuration Used to Evaluate Solution Sensitivity of Small Span Length Control Surface Configurations

Figure 41 represents the spanwise sectional lift variation for k = 1.0 and M = .8 caused by aileron motions for a 9, 13 and 17 downwash chord distribution. The solutions obtained for the 13 and 17 downwash chord analyses are almost identical over the entire span length indicating that converged results may be obtained at least for this configuration using a 13 downwash chord distribution.

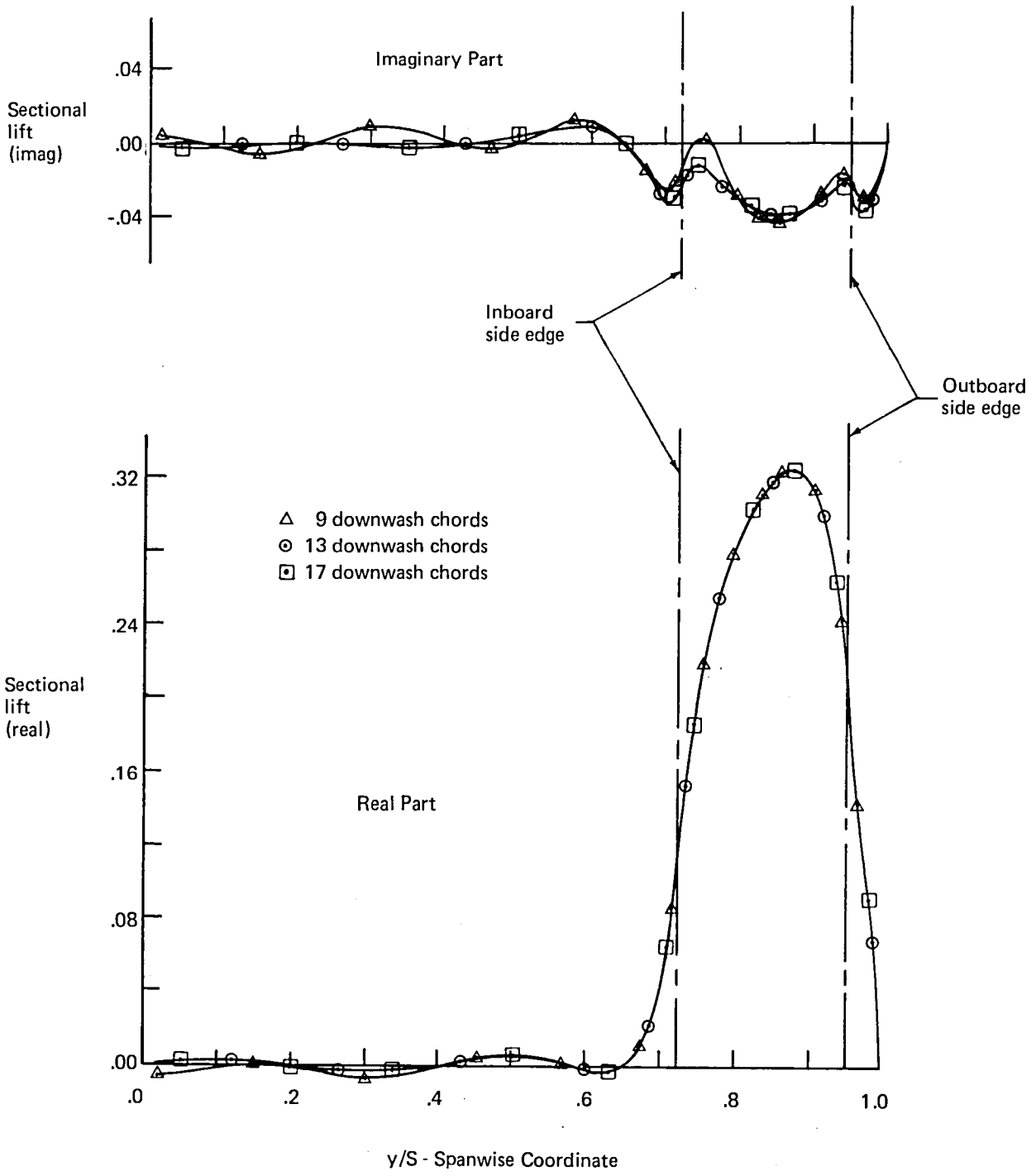

Figure 41.—Real and Imaginary Parts of Spanwise Lift Distribution Due to Aileron Motion at k = 1.0, M = .80

Figure 42 presents the spanwise lift variation due to tab motions at k = 1.0 and M = .8 for analyses using 9, 13 and 17 downwash chords. There are minor variations in results for the 13 and 17 downwash chord analyses which indicate that the solutions are approaching convergence but are not fully converged for the 13 downwash chord.

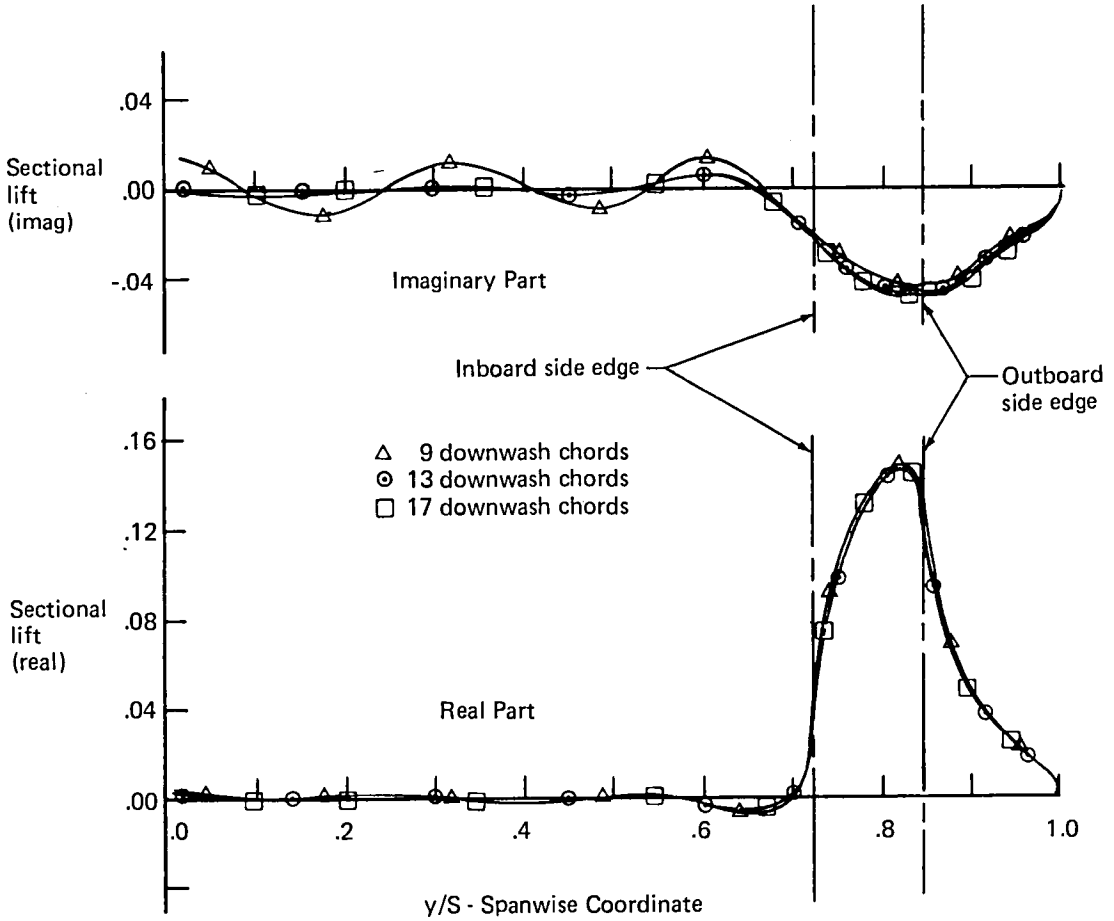

Figure 42.—Real and Imaginary Parts of Spanwise Lift Distribution Due to Tab Motion at k = 1.0, M = .8

Consequently, it should be noted that accurate predictions of unsteady loadings due to motions of small span control surfaces are sensitive to the span lengths of the control surfaces.

Converged solution may be obtained for small span control surface configurations, provided that sufficient care is taken in selecting the proper number of downwash chords to satisfy accuracy requirements.

Table 5 shows the relative reductions in computer costs obtained for small span control surface analyses.

Table 5.—Computer Usage Timing Comparisons Obtained for Small Span Length Control Surface Analysis

				NASA CR-2543 (sec.)	NASA CR-3009 EXTENDED (sec.)	RATIO
13 downwash chords, 5 points per chord	k = 0	Total execution time		171.052	67.139	.393
		Main surface C-matrix	Total	17.234	10.775	.625
			Per DWP	.265	.166	
		Aileron C-matrix	Total	74.304	20.655	.399
			Per DWP	1.143	.456	
		Tab C-matrix	Total	70.761	26.707	.377
			Per DWP	1.089	.411	
	k = 1	Total execution time		477.880	113.667	.238
		Main surface C-matrix	Total	39.720	21.768	.548
			Per DWP	.611	.335	
		Aileron C-matrix	Total	219.492	48.999	.233
			Per DWP	3.377	.753	
		Tab C-matrix	Total	208.891	42.898	.205
			Per DWP	3.214	.660	

CONCLUSIONS

Results of theoretical and numerical investigations to develop economical computing procedures have been applied to an existing computer program that predicts unsteady aerodynamic loadings caused by wing and control surface motions. Improved user flexibility is achieved by increasing computational accuracy and reducing the restrictions on location of downwash stations relative to the leading edge and edges of the control surface boundaries.

Usable analysis range for high Mach number and high k value has been extended to allow greater analysis freedom for high aspect ratio configurations. Computer usage costs are highly dependent upon the geometry of the analysis configuration and on the number and distribution of downwash stations. Comparative results indicate that the revised procedures provide accurate predictions of unsteady loadings as well as providing reductions of 40 to 75 percent in computer usage costs over the previous theoretical program of NASA CR-2543.

REFERENCES

1. W. S. Rowe, M. C. Redman, F. E. Ehlers, and J. D. Sebastian, "Prediction of Unsteady Aerodynamic Loadings Caused by Leading Edge and Trailing Edge Control Surface Motions in Subsonic Compressible Flow-Analysis and Results," NASA CR-2543, August 1975.

2. J. R. Petrarca, B. A. Harrison, M. C. Redman, and W. S. Rowe, "Reduction of Computer Usage Costs in Predicting Unsteady Aerodynamic Loadings Caused by Control Surface Motions–Computer Program Description," NASA CR-145354, June 1978.

3. W. S. Rowe, J. D. Sebastian, and J. R. Petrarca, "Reduction of Computer Usage Costs in Predicting Unsteady Aerodynamic Loadings Caused by Control Surface Motions –Analysis and Results'" NASA CR-3009, March 1979.

4. H. Forsching, H. Triebstein, and J. Wagener, "AGARD-CP-80-71 Symposium on Unsteady Aerodynamics for Aeroelastic Analysis of Intergering Surfaces," Part II, pp. 15-1 to 15-12.

5. B. E. Tinling and J. K. Dickson, "Tests of a Model Horizontal Tail of Aspect Ratio 4.5 in the AMES 12-Foot Pressure Wind Tunnel," NACA RM A9G13, 1949.

6. A. D. Hammond and B. A. Keffer, "The Effect at High Subsonic Speeds of a Flap-Type Aileron on the Chordwise Pressure Distribution Near Mid-Semispan of a Tapered 35° Sweptback Wing of Aspect Ratio 4 Having NACA 65A006 Airfoil Section," NACA RM L53C23, 1953.

7. I. Abel and M. C. Sandford, "Status of Two Studies on Active Control of Aeroelastic Response," NASA TM X-2909, September 1973.

8. A. G. Rainey, C. L. Ruhlin and M. C. Sandford, "Active Control of Aeroelastic Response," AGARD-CP-119, pp. 16-1 to 16-8.

1 Report No	2. Government Accession No	3 Recipient's Catalog No
NASA-CR-145354-1		

4 Title and Subtitle	5 Report Date
Reduction of Computer Usage Costs in Predicting Unsteady Aerodynamic Loadings Caused by Control Surface Motion. Addendum to Computer Program Description	March 1980
	6 Performing Organization Code
7 Author(s)	8 Performing Organization Report No
W. S..Rowe and J. R. Petrarca	
	10 Work Unit No
9 Performing Organization Name and Address	11 Contract or Grant No
Boeing Commercial Airplane Company P. O. Box 3707 Seattle, Washington 98124	NAS1-14122
	13 Type of Report and Period Covered
12 Sponsoring Agency Name and Address	Contractor Report
National Aeronautics and Space Administration Washington, D.C. 20546	14 Sponsoring Agency Code

15 Supplementary Notes

Langley Technical Monitor: Herbert J. Cunningham

Final Report

16 Abstract

This document describes the changes to be made in NASA CR-145354 that will provide increased accuracy and increased user flexibility in prediction of unsteady loadings caused by control surface motions. Analysis flexibility is increased by reducing the restrictions on the location of the downwash stations relative to the leading edge and the edges of the control surface boundaries. Analysis accuracy is increased in predicting unsteady loading for high Mach number analysis conditions through use of additional chordwise downwash stations. User Guidelines are presented to enlarge analysis capabilities of unusual wing-control surface configurations. Comparative results indicate that the revised procedures provide accurate predictions of unsteady loadings as well as providing reductions of 40 to 75 percent in computer usage costs required by previous versions of this program.

17 Key Words (Suggested by Author(s))	18 Distribution Statement
Flutter, Wing-Control-Surface Flutter, Aeroelasticity, Structural Dynamics	FEDD Distribution Subject Category 02

19 Security Classif. (of this report)	20 Security Classif. (of this page)	21 No of Pages	22 Price*
Unclassified	Unclassified	49	

*Available: NASA's Industrial Applications Centers